26
6/10/80 T.S.
237TTS

UCID-18631

MASTER

PRELIMIARY ASSESSMENT OF THE ELECTROMAGNETIC ENVIRONMENT IN THE IMMEDIATE VICINITY OF THE ETA ACCELERATOR

H. S. Cabayan
E. Bogdan
J. Zicker
D. Wythe
G. J. Burke

April 1980

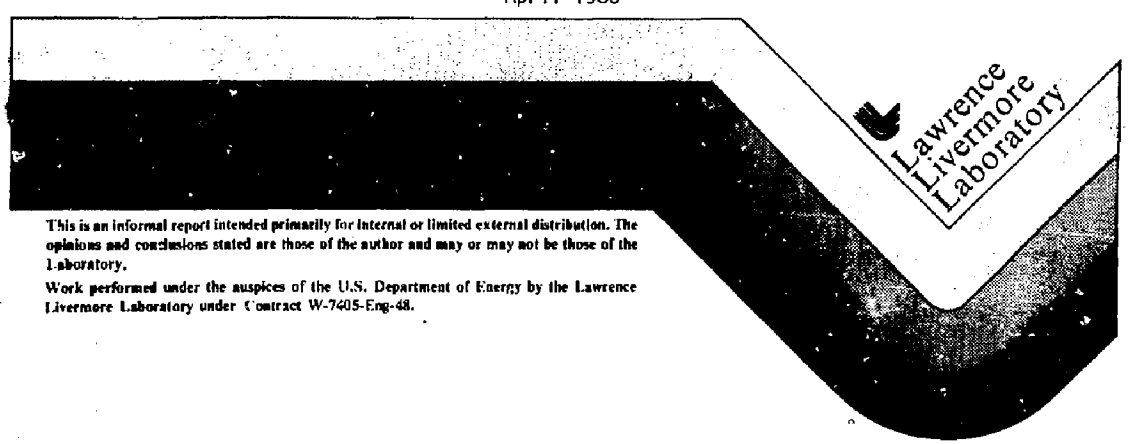

PRELIMINARY ASSESSMENT OF THE ELECTROMAGNETIC ENVIRONMENT IN THE IMMEDIATE VICINITY OF THE ETA ACCELERATOR

H. S. Cabayan, E. Bogdan, J. Zicker, D. Wythe, G. J. Burke

Lawrence Livermore Laboratory

April 1980

ACKNOWLEDGMENT

The authors wish to express their thanks to Bill Barletta and Dick Emmert for their useful suggestions and to Alice Blair, Gail Simpson and Rita Bonivert for typing of the manuscript.

ABSTRACT

The electromagnetic fields in the immediate vicinity of the Experimental Test Accelerator (ETA) at the Lawrence Livermore Laboratory have been characterized. Various EM sensors that cover the frequency band from the very low frequencies up into the GHz region have been used. The report describes in detail the probes, the test set-up and the data processing techniques.

TABLE OF CONTENTS

1.0 INTRODUCTION

This report discusses in detail the techniques used to map the electromagnetic environment in the immediate vicinity of the Experimental Test Accelerator (ETA) at the Lawrence Livermore Laboratory. A variety of EM probes have been used that cover the frequency band from the very low (kHZ) to the very high frequencies (GHz).

The ETA system is briefly described in Section 2.0 where the various sources of ETA emission are qualitatively identified. In Section 3.0, the various sensors used in the measurements are described and their EM characteristics are obtained. Sensor usage and locations are discussed in Section 4.0. The test results are shown in Section 5.0 and discussed in Section 6.0.

2.0 ETA SYSTEM DESCRIPTION

2.1 Physical Layout

The Lawrence Livermore Laboratory has been building an Experimental Test Accelerator (ETA), which is a new linear induction machine incorporating several technological innovations. The ETA will produce a 5 MeV, 10 kA electron beam with an average pulse width of 50 ns with a burst mode of 5 pulses at 1 kHz.[1,2]

The ETA applies a local electric field to a cluster of traveling electrons, accelerating the electrons through the structure. The electrons continuously acquire energy until their total energy is many times their rest energy and their velocity is very close to the speed of light.

Illustrated in Figure 1 is the ETA model consisting of four major sections: a pulse-forming network, cathode injector gun, post-accelerator, and an experimental tank.* The post-accelerator that contains the non-resonant cavities is the heart of the linear accelerator. A relatively low-energy beam is injected into the post-accelerator by the electron injector gun. Once the beam is at its final energy at the terminal end of the post-accelerator, it is magnetically guided in the beam transport unit to an experimental area.

Pulsed electrical power for the accelerator is provided by a pulse-forming network, which performs the process of energy compression. A discrete amount of energy is stored in a series of components over a period of time and is released suddenly. An example of a storage component is an electrical transmission line that is charged to a desired voltage in much the same manner as a capacitor. A cylindrical three-conductor transmission line (Blumlein)[3,4] is used in the pulsed electron ETA.

The power conditioning diagram in Figure 2 demonstrates the actual conversion of energy from primary ac power to the beam. The ac power drives an energy-storage and charging network. The latter delivers a high voltage pulse that is stepped up to 250 kV by a resonant transformer bolted to the Blumlein transmission line. Shortly after the current that

* At the time the data shown in this report was taken, the metal tank had not yet been installed. The beam hit a target at the end of the beam transport unit.

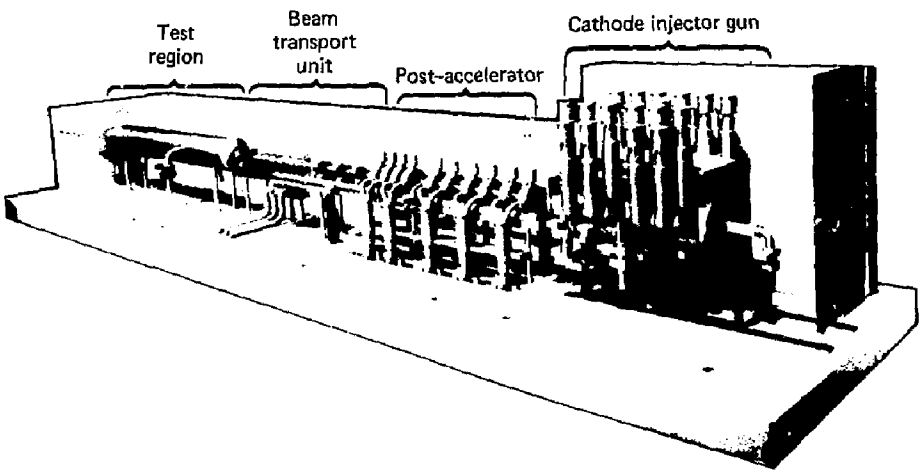

FIGURE 1 Experimental Test Accelerator (ETA)

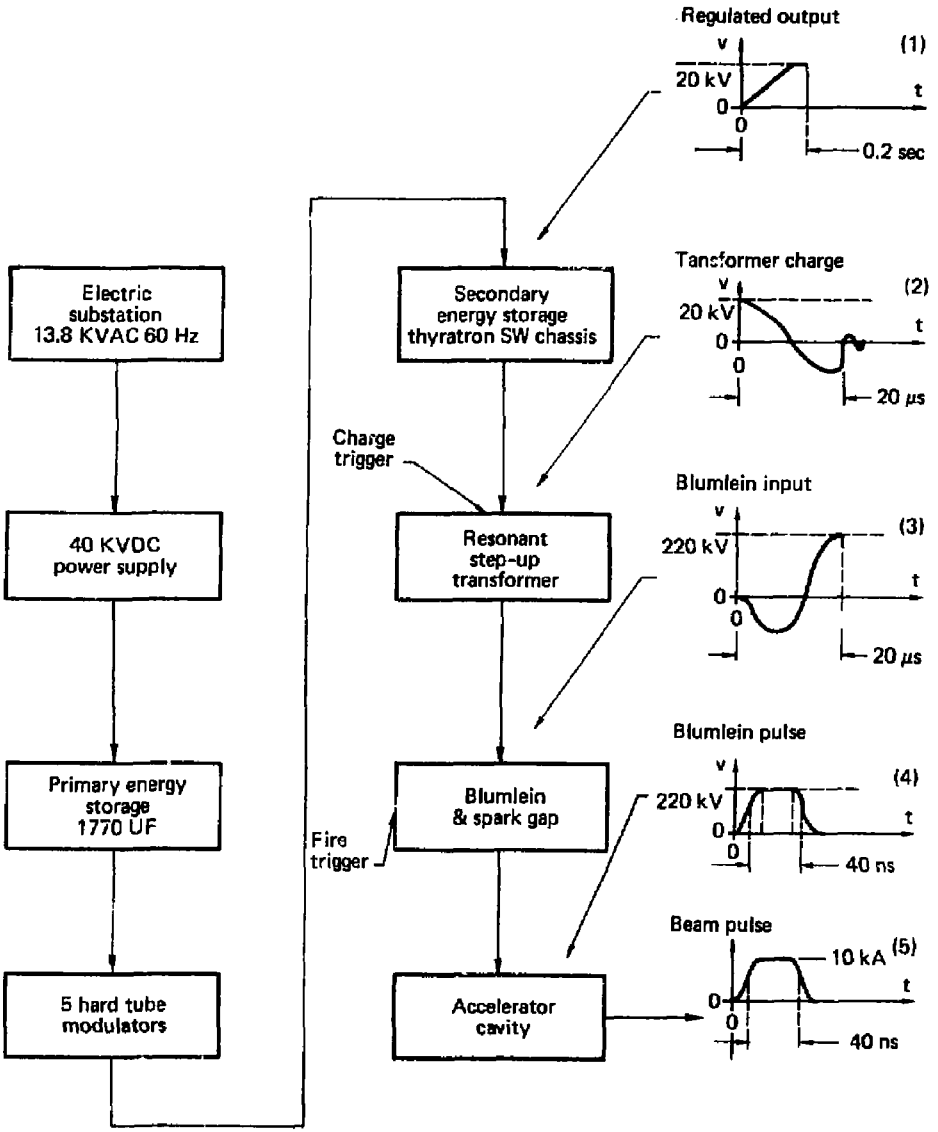

FIGURE 2 Power Conditioning Diagram

charged the Blumlein has dropped to zero, the spark gap switch is fired by a 150 kV trigger circuit. The resultant high-voltage output of the Blumlein is now impressed across the accelerating gap. The accelerating gap is formed by an axially symmetric metallic structure that encloses toroidal cores of ferromagnetic material (Figure 3). The ferrite acts as a large inductance, initially preventing a large current from flowing through the structure around the ferrite, preventing the shorting of the coaxial line. For the duration of this pulse, electrons passing the gap will be accelerated. The energy that took 20 μs to store in the Blumlein is delivered to the accelerating cavity in 50 ns.

Accelerating voltages in both the cathode injector and the post-accelerator are provided by similar power-supply and pulse-forming networks feeding the ferrite induction cores.

A schematic cross section of the cathode injector gun is shown in Figure 4. It is constructed in two parts, each with five 250 kV induction units in series. After emerging from the gun, the electron beam passes sequentially through 10 modular accelerating units fed by Blumleins. Each unit adds 0.25 MeV of kinetic energy to the beam, and a final energy of 5 MeV per particle is acquired.

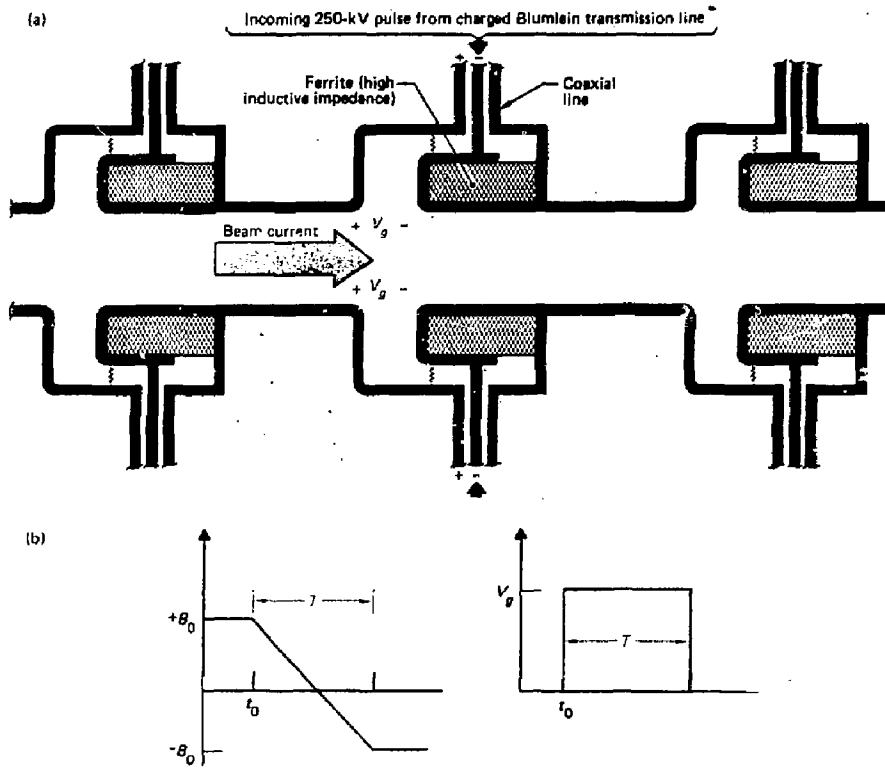

FIGURE 3 Schematic Representation of Accelerating Gaps

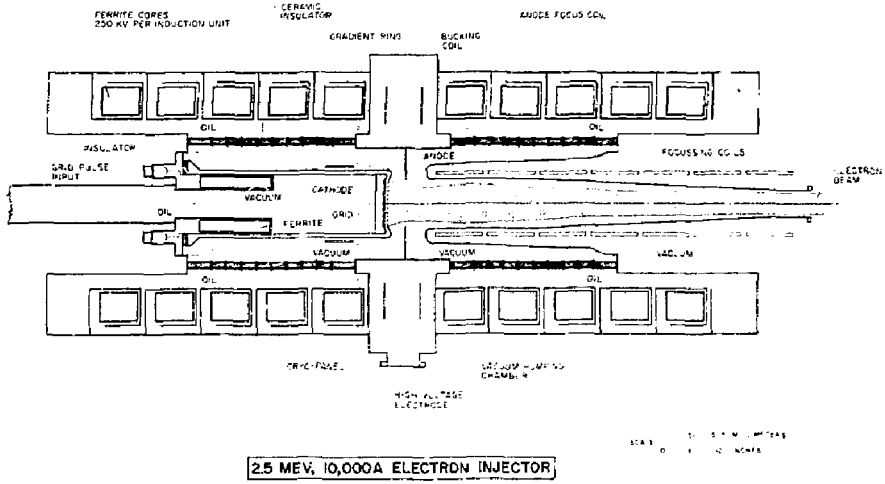

FIGURE 4 ETA Electron Gun Injector

2.2 Potential EM Sources

Most of the stages shown in the power conditioning diagram in Figure 2 are potential sources of EM radiation from the accelerator. These will have varying degrees of radiation capabilities depending on the amount of shielding between the sources and the environment around the accelerator. The various ETA units shown in Fig. 1 operate at very low pressures and therefore the presence of the apertures for significant EM radiation on these units is highly unlikely. However the hundreds of cables linking the accelerator to the electric power sources are potentially good sources of EM radiation. The various stages in Figure 2 are probably not 100% isolated from each other and therefore EM energy can be reflected and flow backwards from the forward sections to the initial stages which are usually not as tightly shielded as the forward sections. Even though this less than 100% tight EM shielding on the initial stages does not affect the usual operation of the ETA, it does allow for emission of EM energies of all frequencies into the environment around the accelerator, and which are high enough to be detected.

The time dependent waveshapes at the successive stages are numbered from 1 to 5 in Figure 2. At the time the data shown in this report was taken, the ETA was in the process of final construction and testing and the actual waveshapes did not correspond exactly to those shown in Figure 2. However, for the purposes of a qualitative discussion in this section, reference will be made to these figures.

The slow risetime of waveshape #1 will give rise to very low frequencies (in the Hz) which cannot be easily detected. Waveshape's #2 and 3 have frequency contents in the kHz up to a few MHz. Frequencies above 10 MHz are to be expected from the last two time histories. Another source of EM energy are the spark gaps which tend to be quite noisy. Separate spark gap measurements have indicated that these are capable of producing frequency components around 50 MHz and above. These various EM sources will excite the whole ETA structure which in turn will re-radiate EM energy at frequencies corresponding to its structural resonances. These are discussed in Appendix A.

3.0 SENSOR CHARACTERISTICS

In this section, the various probes used will be described and their EM characteristics will be obtained. The calibration functions relating the received voltage to the incident electric or magnetic field will be shown either in equation form or with a plot. These are obtained either analytically (whenever possible) or with appropriate tests.

3.1 Electric Field Sensors

Four electric field probes were used. The first two (the EG&G and the LLL monopole probes) are small in size but very broadband. The small size limits the sensitivity. They are ideal when large signals are available. The next two probes have higher sensitivities and cover the frequency band from 1 MHz on up into the GHz region. The LLL Active Antenna has an almost flat response from 2 MHz up to 20 MHz. The Log-Periodic Antenna covers the frequency band from 20 MHz on up. These antennas will now be separately described.

3.1.1 EG&G Electric Field Probe

This is a small electric field sensor. A close-up view is shown in Figure 5. It is a specially shaped monopole placed above a small plate that acts as a ground plane. It is enclosed within a plastic cover for protection purposes. The special shaping yields an exact determination of the monopole capacitance to ground. Because of its small size, it basically acts as a capacitive probe up into the GHz region and above. Some pertinent parameters of this probe are listed below:

Physical Height of Monopole:	6.7 mm
Capacitance to Ground (C):	.344 pf
Electrical Effective Area (A):	$10^{-4}m^2$
Electrical Effective Height (h):	2.57 mm

The equivalent circuit of this probe is given in Figure 6. The current source i(t) is the product of the capacitance, the effective height and the time derivative of the electric field. The shunt impedances consist of the capacitance of the antenna in parallel with the 50-Ω receiver load. At the frequencies of interest, the antenna load impedance $1/\omega C$ is much larger than the 50-Ω receiver load impedance, and with very good approximation, the receiver voltage is given by:

$$V(t) = ChR_L\dot{e}(t)$$

$$= \varepsilon_0 AR_L\dot{e}(t) \text{ (since } Ch=\varepsilon_0 A,\ \varepsilon_0=8.854\times10^{-12})$$

In the frequency domain, the electric field $E(\omega)$ is therefore given in terms of the received voltage $V(\omega)$ by the following expression

Figure 5. Close-up View of EG&G Electric Field Sensor

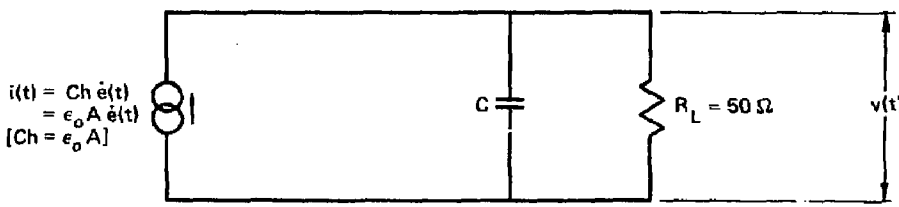

FIGURE 6 Equivalent Circuit of EG&G Electric Field Probe

$$E(\omega) = T(\omega) \cdot V(\omega)$$

where $$|T(\omega)| = \frac{1}{\omega \varepsilon_0 A R_L} = \frac{3.6 \times 10^{12}}{f}$$

Hence, the transfer function is inversely proportional to the frequency. This expression is valid for frequencies up into the GHz region.

3.1.2 LLL Monopole Probe

The principle of operation of this probe is the same as the one described in the previous section. The difference is that it is smaller in size and therefore has higher sensitivity. Its effective area is about 3 times larger than the EG&G probe and its transfer function is correspondingly lower by a factor of 3. Even though its capacitance is somewhat larger, it still does not appreciably load the circuit for frequencies below the GHz range. A view of this antenna is shown in Figure 7.

3.1.3 LLL Active Antenna

This LLL constructed antenna is a capacitive loaded short dipole connected to a very high impedance FET amplifier. The FET amplifier is connected to a Darlington transistor pair as a line driver output circuit. Both the amplifier/line driver and the dipole probe are housed in a 46 by 5 cms diameter teflon and metal cylinder case.

This antenna was calibrated in a parallel plate simulator shown in Figure 8. A TEM wave is launched between the plates with electric field vector parallel to the axis of the antenna. The induced voltage at the

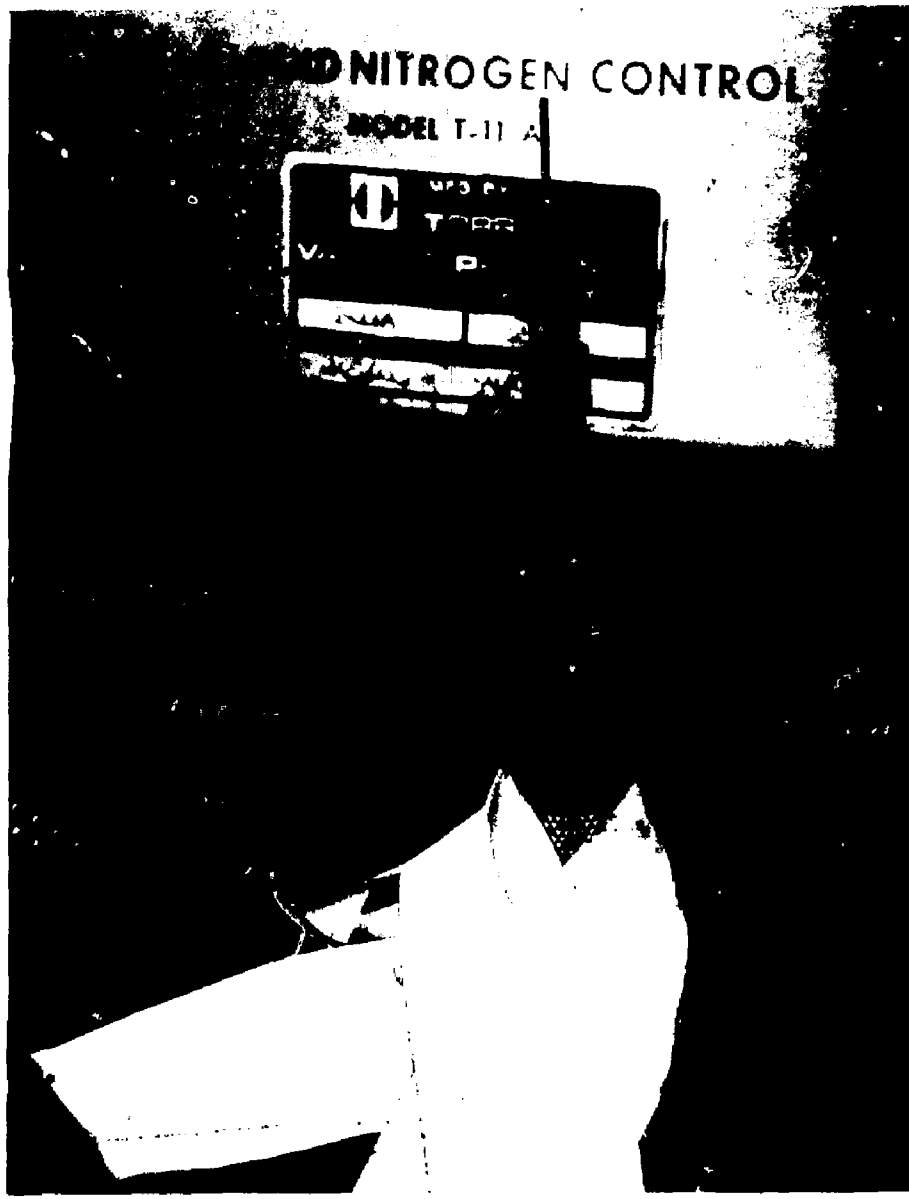

Figure 7. Close-up View of LLL Monopole Probe

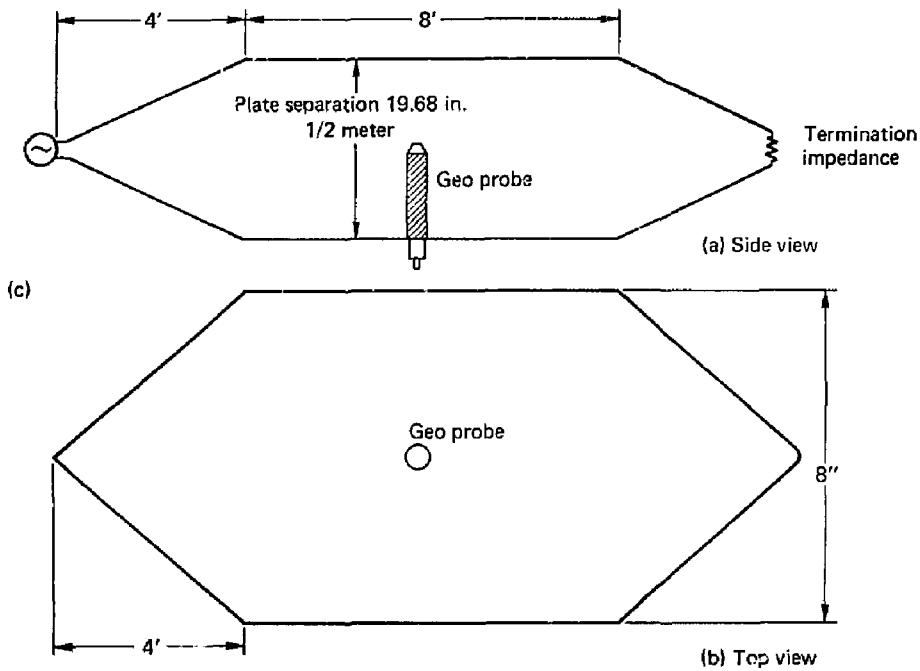

FIGURE 8 Schematic Representation of Test Set-Up for Calibrating LLL Active Antenna

antenna termination is measured and the transfer function is computed. This is done at a larger number of frequencies within the operating band of the antenna. The 3 db bandwidth frequencies were measured to be 275 kHz and 19 MHz. In the flat portion of the response curve, the transfer function is unity (i.e., a 1 V/m incident field induces a voltage of 1 V across the antenna terminals). The antenna was also tested for its linearity characteristics. It was found that it was 100% linear for peak received voltages up to ± 1 V. A photograph of this antenna is shown in Figure 9. It is mounted on the top of a wooden support inside the ETA building.

3.1.4 Log-Periodic Antenna

This device is a 30 element log-periodic antenna manufactured by American Electronic Lab (model AEL-APN-1509). A view of this antenna mounted for horizontal polarization is shown in Figure 10. The manufacturer of the antenna had provided both the gain and the VSWR as a function of frequency. However, that information was not sufficient to determine the transfer function relating the incident electric field to the received voltage. This transfer function was determined numerically for the frequency band from 10 to 100 MHz. The details of the modeling are given in Appendix B. In Figure B2 of this appendix, the solid curve gives the magnitude of the induced voltage across the antenna terminals as a function of frequency for a 1 V/m-Hz incident electric field incident from the forward direction with a polarization vector parallel to the antenna elements. The dashed line in the same figure is a linear approximation. Using the equation of this line, the following is an approximate equation relating the incident field to the received for the frequency range from 20 to 100 MHz:

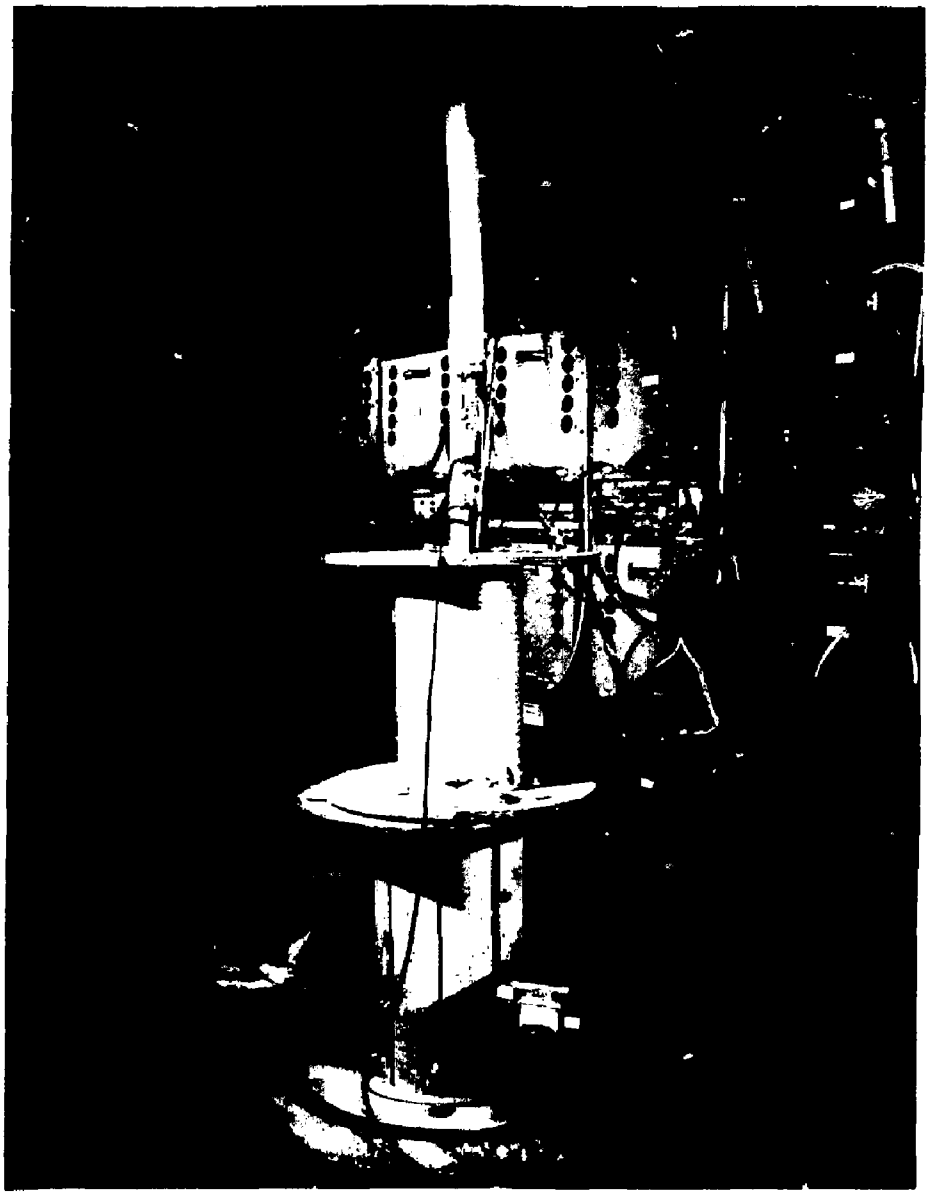

Figure 9. View of LLL Active Antenna

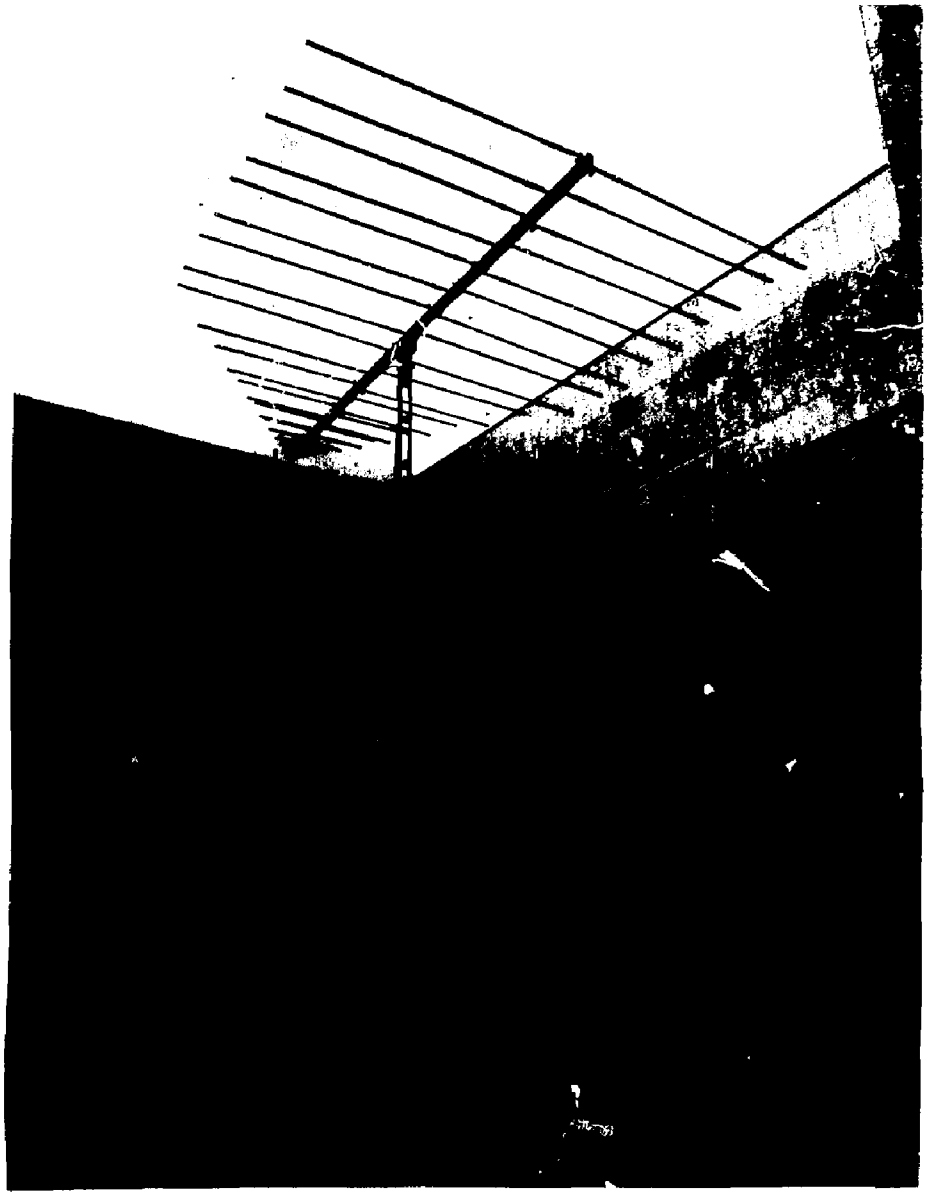

Figure 10. View of 30 Element Log Periodic Antenna

$$E(\omega) = T(\omega)V(\omega)$$

$$|T(\omega)| = \frac{1}{2.22 - .019f} V(\omega) \quad [f \text{ in MHz}]$$

3.2 Magnetic Field Probes

Two magnetic field probes were used. The first one is a small sized probe manufactured by EG&G that is mounted flush against a flat metal surface. It thus measures the fields (and therefore the surface currents) right on these surfaces. This probe has very broadband characteristics with improved sensitivity at the higher frequency. For the lower frequency, a multi-turn loop antenna is used.

3.2.1 EG&G Magnetic Field Probe

A close-up view of this probe is shown in Figure 11. It is manufactured by EG&G (Model MGL-S7A(R)). Because of its small size, it acts as an inductive probe up into the GHz region. Some pertinent parameters of this probe are listed below,

Electrical Effective Area (A): 10^{-4} m^2

Inductance (L): 7.07 nH

The equivalent circuit is given in Figure 12. The voltage source v(t) is the product of the free space permeability, the effective area and the time derivative of the magnetic field. Up to a frequency of about 1 GHz, the series impedance of the antenna is negligible with respect to the load impedance R_L. In the time domain, the received voltage is therefore given by

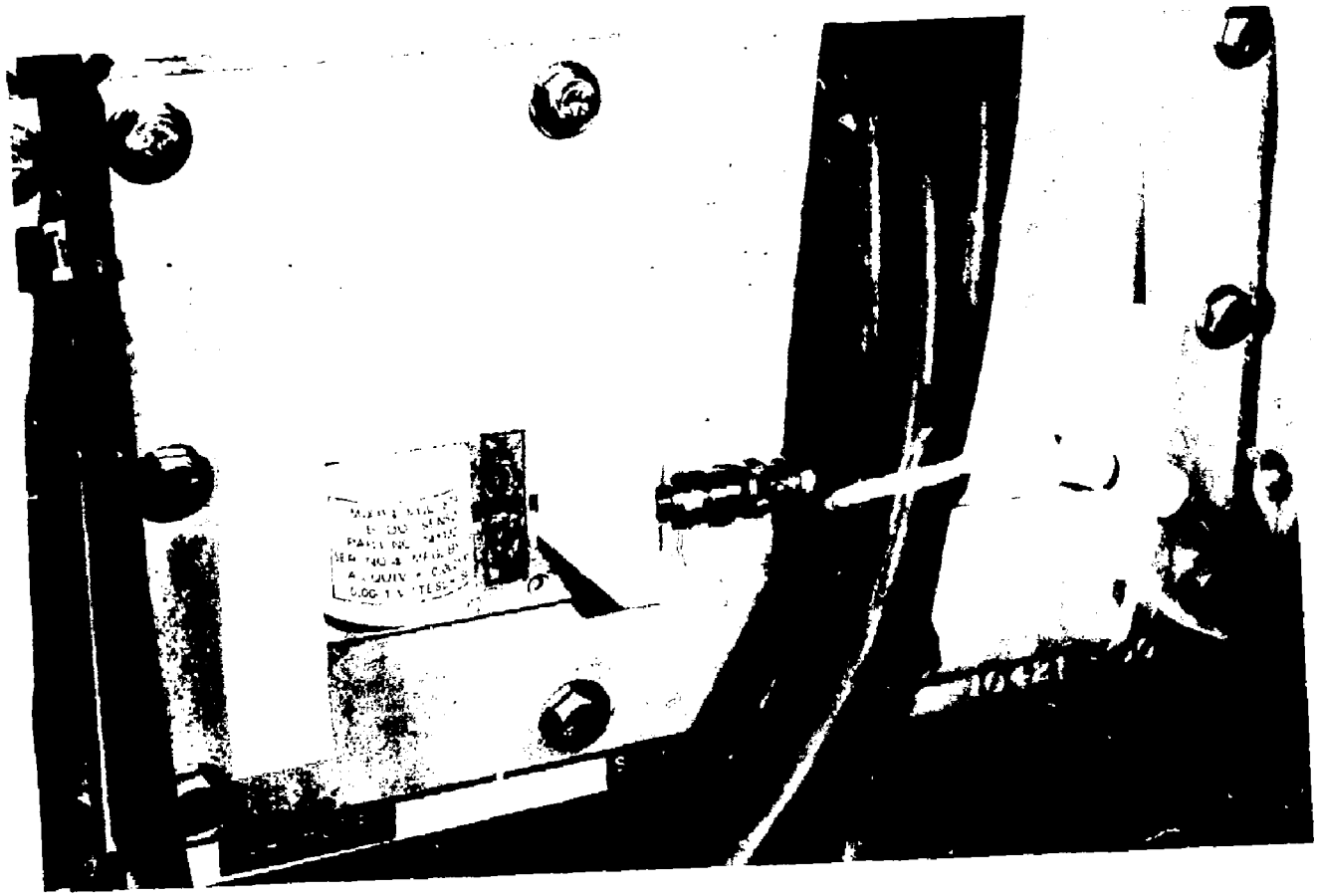

Figure 11. Close-up View of EG&G Magnetic Field Probe

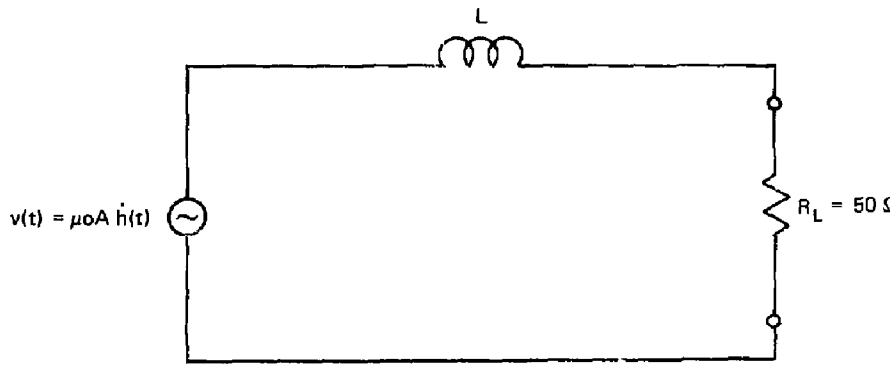

FIGURE 12 Equivalent Circuit of EG&G Magnetic Field Probe

$$v(t) = \mu_o A \dot{h}(t)$$

In the frequency domain, the magnetic field $H(\omega)$ is given in terms of the received foltage $V(\omega)$ by the following expression

$$H(\omega) = T(\omega)V(\omega)$$

where

$$|T(\omega)| = \frac{1}{\mu_o A \omega} = \frac{1.3 \times 10^9}{f}$$

This expression is valid for frequencies up to about 1. GHz.

3.2.2 Loop Antenna

This LLL manufactured loop sensor covers the frequency range up to ~15 MHz. A close-up view of this probe is shown in Figure 13. The physical descriptions of this loop and its electrical properties follow:

- Loop Diameter: 24"
- Loop Coil: 16 turns of #22 wire
- Effective Area* A: 4.7 m^2
- Loop Inductance**: ~500 μH (measured)
- Loop radius r: .3 m

* The Effective Area $A = n \cdot \pi r^2$, where n is the number of turns.

**The inductance of the Loop $L = n^2 r \mu_o [\ell n \frac{8r}{a} - 2]$ henry, where $\mu_o = 4\pi \times 10^{-7}$. This gives an inductance of 680 μh. The loop inductance, however, was measured to be 500 ± 6 μh. The measured value was used in making transfer function calculations.

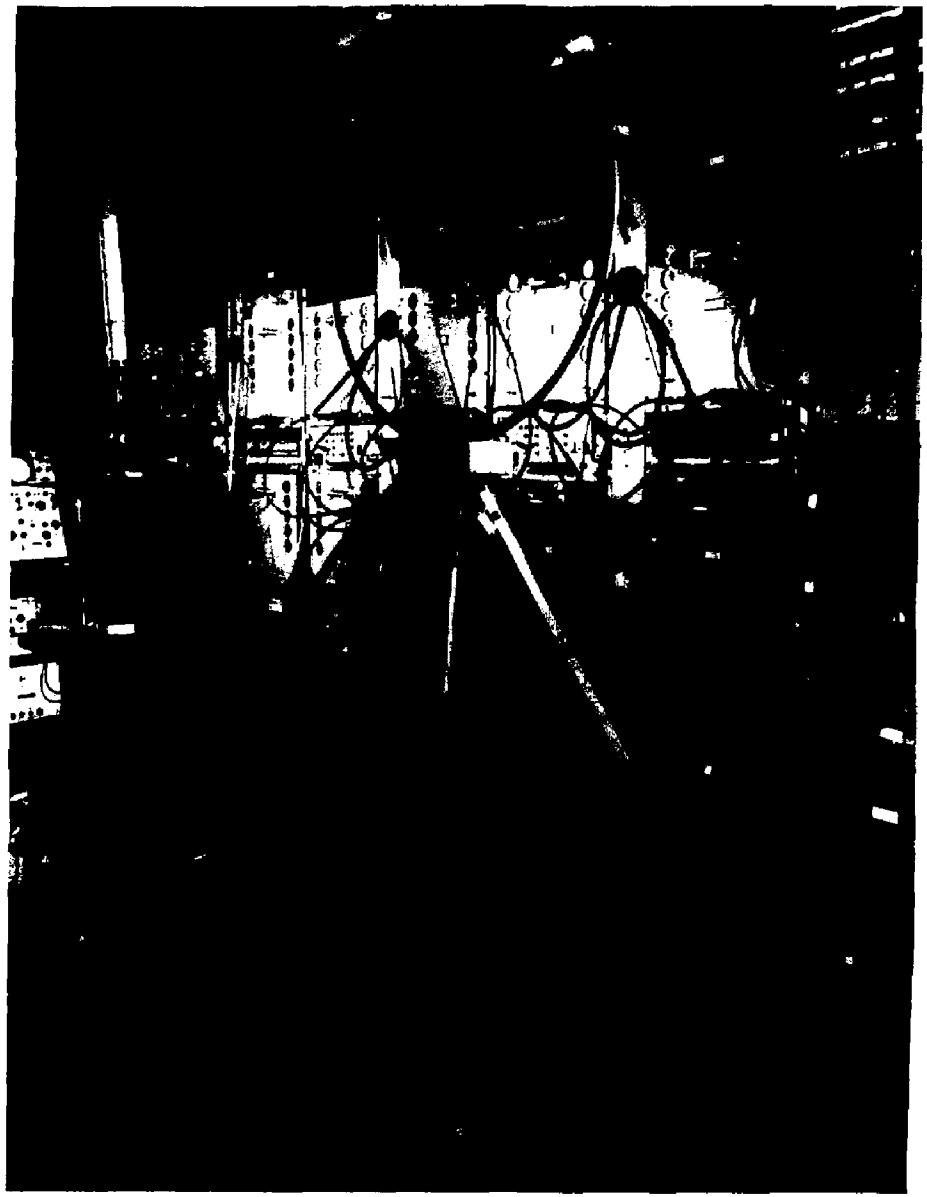

Figure 13. View of LLL Loop Antenna

The equivalent circuit of this probe is the same as the one developed for the EG&G magnetic field probe in Figure 12. This simple equivalent circuit is valid only up to frequencies where the diameter of the loop is less than a 1/10 of a wavelength. This limits the validity of the model to frequencies less than 15 MHz. In this frequency range, the series impedance of the loop cannot be neglected with respect to the load impedance R_L. In the frequency domain, the magnetic field $H(\omega)$ is given in terms of the received voltage $V(\omega)$ by the following expression

$$H(\omega) = T(\omega)V(\omega)$$

$$\text{where} \quad |T(\omega)| = \frac{2.7 \times 10^4}{f} \left|1 + j\, 2\pi \times 10^{-5} f\right| \quad (f \leq 15 \text{ MHz})$$

3.3 Cable Current Probe

This probe manufactured by GENISCO (type GCP 5130A-SERIAL No. 159) was used to measure currents on cables connecting the various electrical stages of the accelerator. The voltage (V) induced across the terminals of the probe is related to the current (I) on the cable through a transfer impedance Z_T,

$$V(\omega) = Z_T(\omega) I(\omega).$$

A plot of the transfer impedance is provided by the manufacturer and given in Figure 14. It covers the frequency range from 1 kHz to 100 MHz. The transfer function that relates the current to the probe voltage is given by

$$T(\omega) = \frac{1}{Z_T(\omega)}$$

If the curve in Figure 14 is approximated by the dashed line, then:

$$T(\omega) = 80 \times 10^{-2.6f/10^6} \qquad (f < 1 \text{ MHz})$$

$$= .2 \qquad (f > 1 \text{ MHz})$$

where f is in Hz.

3.4 Summary of Sensor Characteristics

The characteristics of all sensors used in the measurements are summarized in Table 1. The transfer functions and their corresponding ranges of validity are listed in columns 3 and 4 respectively.

4.0 SENSOR USAGE AND LOCATIONS

The various probes described in the previous sections were placed on the ETA and in the immediate vicinity (both inside the building that houses the machine and outside of it). In order to measure the surface currents and electric fields on the ETA machine, electric and magnetic field probes were used. In addition, the current flowing in a cable connected to the ETA (in this case, a Blumlein charging cable) was monitored with the current probe. Other probes were used to monitor both the electric and magnetic fields in the immediate vicinity. The reason for probes being placed on the machine itself is to avoid possible problems in interpreting the data. The fields and currents on the ETA are very large in magnitude and therefore all observed resonances can be attributed without much doubt to the ETA. All resonances observed in the fields measured around the ETA should necessarily correspond to those measured on the ETA. Therefore, any interfering signals from other sources can be easily identified. Furthermore, the fields and currents on the ETA are useful in another way; they allow one to make quick estimates of the fields at a distance from the ETA. The ETA can be roughly modeled in an EM sense as a fat cylinder and radiated fields from such cylinders can be adequately evaluated.

TABLE 1. SUMMARY OF SENSOR CHARACTERISTICS

TYPE		TRANSFER FUNCTION (Frequency f in Hz)	RANGE OF VALIDITY OF TRANSFER FUNCTION
Electric Field Probe	EG&G Electric Field Probe	$E(\omega) = T(\omega)V(\omega)$ $\lvert T(\omega)\rvert = 3.6\times10^{12}/f$	Up into GHz region
	LLL Monopole Probe	$E(\omega) = T(\omega)V(\omega)$ $\lvert T(\omega)\rvert = 1.2\times10^{12}/f$	Up into GHz region
	LLL Active Antenna	$E(\omega) = T(\omega)V(\omega)$ $\lvert T(\omega)\rvert = 1$	3 db Bandwidth: 275 kHz - 19 MHz
	Log-Periodic Antenna	$E(\omega) = T(\omega)V(\omega)$ $\lvert T(\omega)\rvert = 1/(2.22-.019\times10^{-6}f)$	20 - 100 MHz
Magnetic Field Probe	EG&G Magnetic Field Probe	$H(\omega) = T(\omega)V(\omega)$ $\lvert T(\omega)\rvert = 1.3\times10^{9}/f$	Up into GHz region
	Loop Antenna	$H(\omega) = T(\omega)V(\omega)$ $\lvert T(\omega)\rvert = \frac{2.7}{f}\times10^{4}\lvert 1+j2\pi\times10^{-5}f\rvert$	$f \leq$ MHz
Cable Current Probe		$I(\omega) = T(\omega)V(\omega)$ $\lvert T(\omega)\rvert = 80\times10^{-2.6f/10^{6}}$ ($f <$ 1 MHz) $= .2$ ($f \geq$ 1 MHz)	1 kHz - 100 MHz

NOTE:

$H(\omega)$: Magnetic Field in frequency domain (A/m-Hz).

$E(\omega)$: Electric Field in frequency domain (V/m-Hz).

$V(\omega)$: Induced Voltage at antenna terminals in frequency domain (V/Hz).

$I(\omega)$: Cable Current in frequency domain (A/Hz).

f: Frequency in Hz.

A simplified plan view of the ETA building including probe locations is shown in Figure 15. [See detailed sketches in Appendix C.] The following numbering system is used to denote the various probes

P1: EG&G Electric Field Probe

P2: LLL Monopole Probe

P3: LLL Active Antenna

P4: Log-Periodic Antenna

P5: EG&G Magnetic Field Probe

P6: Loop Antenna

P7: Cable Current Probe

Probes P2 and P5 were placed at the cathode end of the ETA to monitor the normal electric and magnetic fields (i.e., axial surface currents) on the surface of the ETA. This is a region which is relatively free of x-ray and therefore the probe response is due to the electromagnetic fields only. P2 and P5 were placed approximately 30" and 45" from the end of the cathode case respectively [see Appendix C]. P1 was placed at the other end of the machine towards the beam target port. Layers of lead brick were used to insulate the probe from the x-rays emitted at the target. This probe monitors the vertical electric fields in the target region.

Probes P3 and P6 were placed at two different locations. In Figure 13, a view of these probes is shown when inside the ETA building. The view of the probes placed outside the building is shown in Figure 16. Probe P3 monitors the vertical electric fields and P6 the magnetic fields normal to its surface. The log-periodic antenna (P4) was placed outside the building because of its

FIGURE 15 Plan View of ETA and Probe Locations

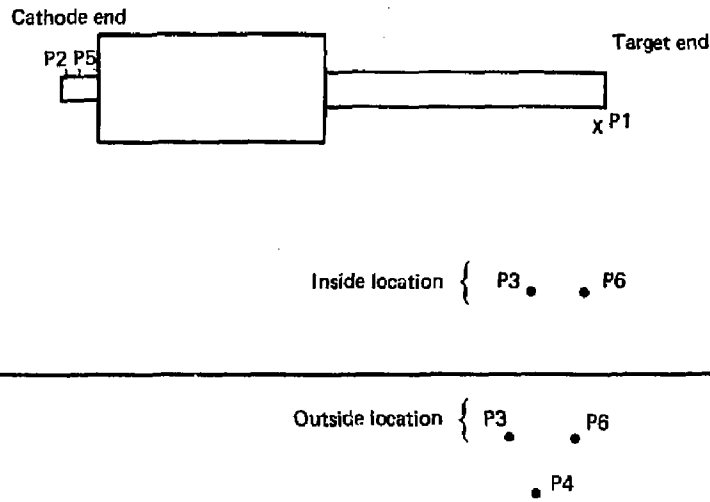

Note
P1: EG&G Electric field probe
P2: LLL Monopole probe
P3: LLL Active antenna
P4: Log Periodic antenna
P5: EG&G Magnetic field probe
P6: Loop antenna

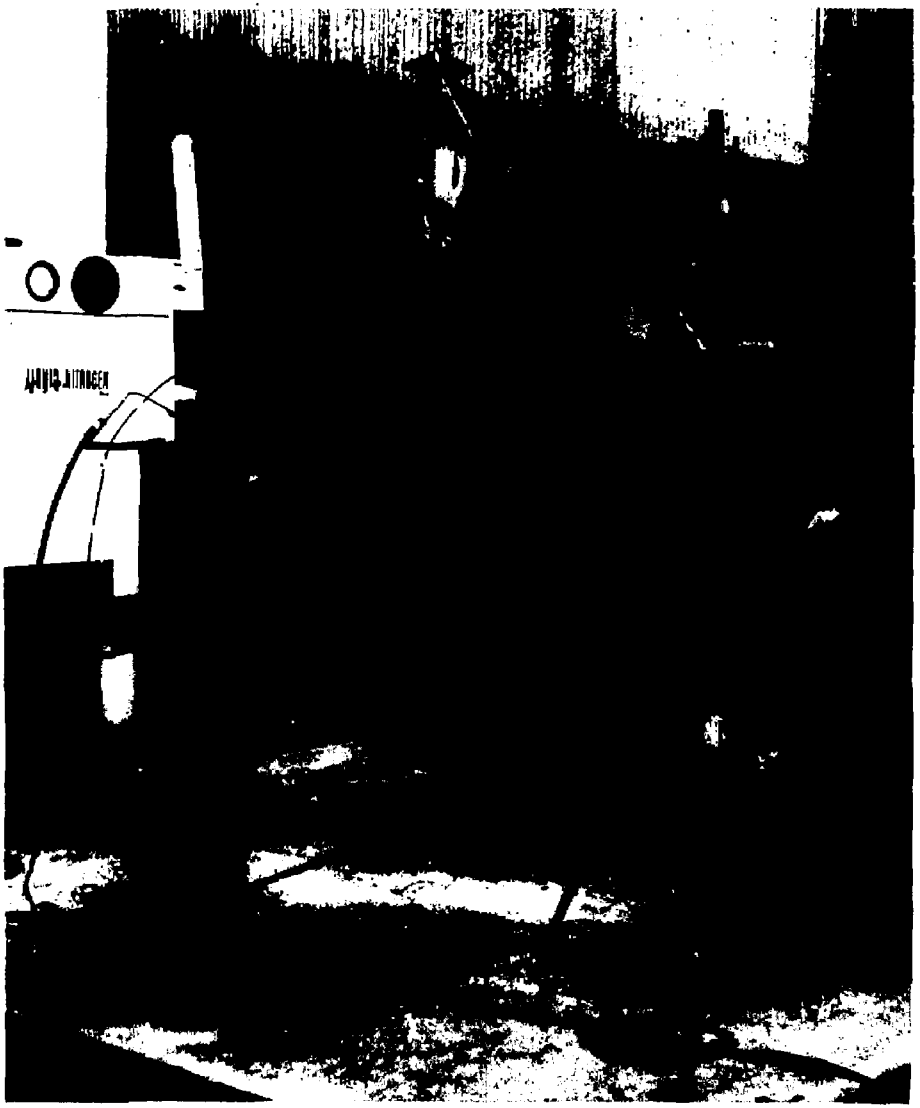

Figure 16. View of LLL Active Antenna and Loop Antenna Positioned Outside ETA Building

large size. A view of the antenna when positioned to respond to horizontally polarized fields is shown in Figure 10. Measurements were also taken with the antenna in a vertical position to monitor vertically polarized electric fields.

The current probe was placed around a master Blumlein charging cable located on the upper deck of the building.

All received signals from the sensors were brought into a shielded instrument room where they were recorded and processed. The data acquisition and processing techniques are described in Appendix D.

5.0 TEST RESULTS

The time histories of all signals from the various probes were recorded and the Fourier transforms obtained [see Appendix D for details]. The appropriate transfer functions which were stored in the minicomputer were used to calibrate the frequency plot of the electric and/or magnetic fields. The validity of the frequency data was confined to the lower and upper bounds provided by the length of the time record of the recorded waveshape and the number of sample points. For example, if the maximum time record is T, then the lower bound f_{min} is 1/T and the upper bound f_{max} is $\frac{N}{2T}$ where N is the number of sample points.

In this report, data is shown for frequencies up to 100 MHz. Except for the LLL active antenna and the loop antenna, all other antennas cover this range adequately. The range of validity of the loop is 14 kHz to 150 kHz and for the active antenna it is up to 19 MHz. For the set of measurements reported here, no active antenna data is included since it was found to have saturated after the data was taken. The transfer function of the log-periodic antenna was evaluated down to 2 MHz [see Appendix B] and this limits the lower bound on the validity of the transformed data from this antenna.

In Table 2, the representative set of data shown in this section are tabulated. For each entry, the following information is given

TABLE 2. LIST OF TEST DATA AND PERTINENT CHARACTERISTICS

DATA #	FIELD TYPE	PROBE *	T μs	f_{min} MHz	f_{max} MHz	Beam (on,off)	Trigger (Charge,Fire)	Fig. #
1	Electric	P1	0.5	2.0	512.0	On	Fire	17,18
2	Electric	P2	50.0	0.02	5.12	Off	Charge	19
3	Electric	P2	2.0	0.5	128.0	Off	Fire	20,21
4	Electric	P2	2.0	0.5	128.0	On	Fire	22,23
5	Electric	P4 (1)	0.5	2.0	100.0	Off	Fire	24,25
6	Electric	P4 (1)	4.0	2.0	100.0	On	Charge	26,27
7	Electric	P4 (1)	0.5	2.0	100.0	On	Fire	28,29
8	Magnetic	P5	0.5	2.0	512.0	On	Fire	30,31
9	Magnetic	P6 (2)	10.0	0.1	15.0	Off	Charge	32,33
10	Magnetic	P6 (2)	50.0	0.02	5.12	Off	Charge	34,35
11	Magnetic	P6 (3)	0.5	2.0	15.0	On	Fire	36,37
12	Current	P7	50.0	0.02	5.12	On	Fire	38,39

(1): Log-Periodic in horizontal position.
(2): Loop inside ETA building.
(3): Loop outside ETA building.

*P1: EG&G Electric Field Probe.
P2: LLL Monopole Antenna
P4: Log-Periodic Antenna
P5: EG&G Magnetic Field Probe
P6: Loop Antenna
P7: Cable Current Probe

1 - type of probe:	P1 to P7 (see Figure 15)
2 - T:	duration of time record
3 - f_{min}:	lower bound on valid frequency range
4 - f_{max}:	upper bound on valid frequency range
5 - Beam:	beam information; whether on or off
6 - Trigger:	trigger information; whether charge (Blumlein charging) or fire (Blumlein discharging)
7 - Figure #:	Appropriate Figure #'s for the time and frequency domain

The lower and upper bounds in items 3 and 4 above are due to either antenna limitations or limitations in the transfer functions used. For those cases when f_{max} > 100 MHz, data up to ~100 MHz is shown. The initial test plans called for recording data with each probe with the beam off and on and for each probe with the trigger set at charge and discharge. At the completion of the tests, some of the data records could not be used which explains the incomplete nature of the entries in Table 2.

The time and frequency plots for data numbers 1 to 12 are shown in Figures 17 to 39. The time histories correspond to the voltages induced at the probe terminals. The frequency domain curves have been transformed with the appropriate transfer function and therefore give the electric field in V/m-Hz, magnetic field in A/m-Hz, or current in A/Hz as the case may be. In all cases, the vertical axes of frequency plots are given in dB with respect to unity. It should be added that the data was taken over an almost three-week period when the ETA was being tested. It is very likely that the machine characteristics were changing and therefore will be reflected in the data giving rise to some inconsistencies both in amplitude and frequency variations.

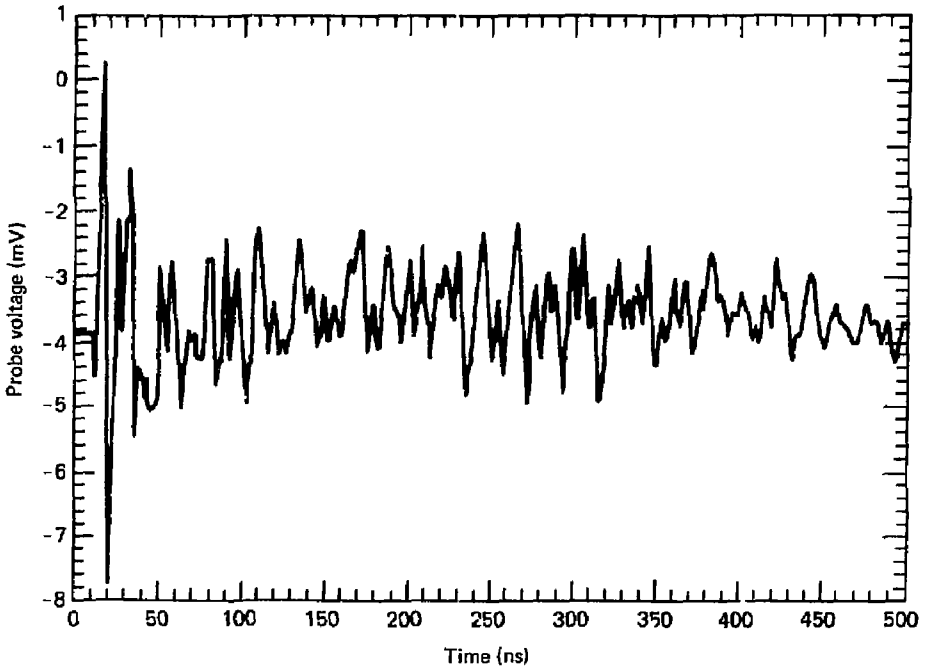

FIGURE 17 Time Domain Plot of Electric Field

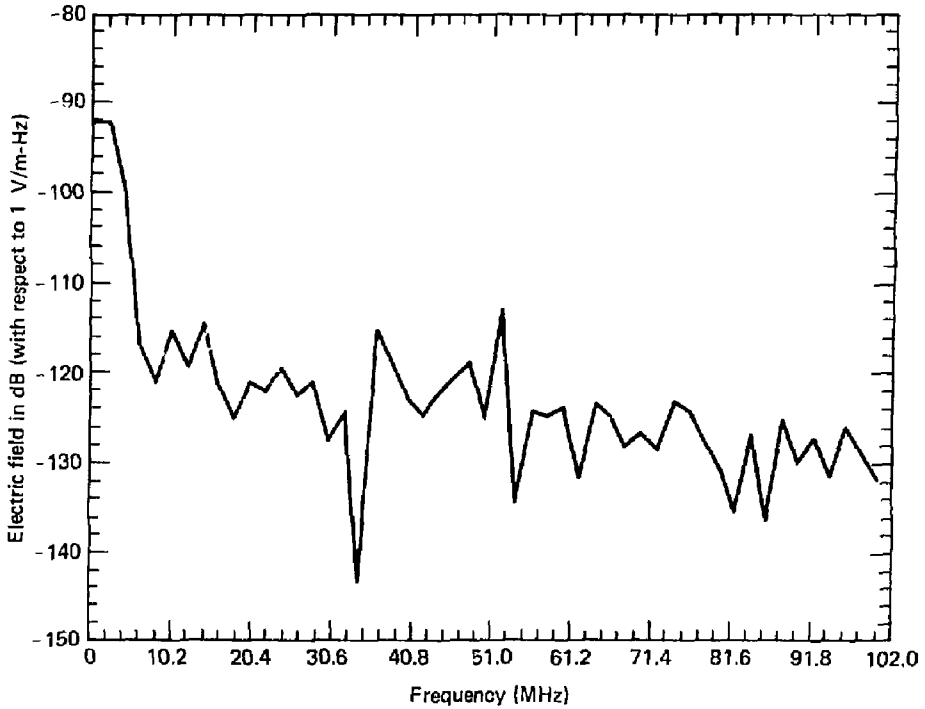

FIGURE 18 Frequency Domain Plot of Electric Field

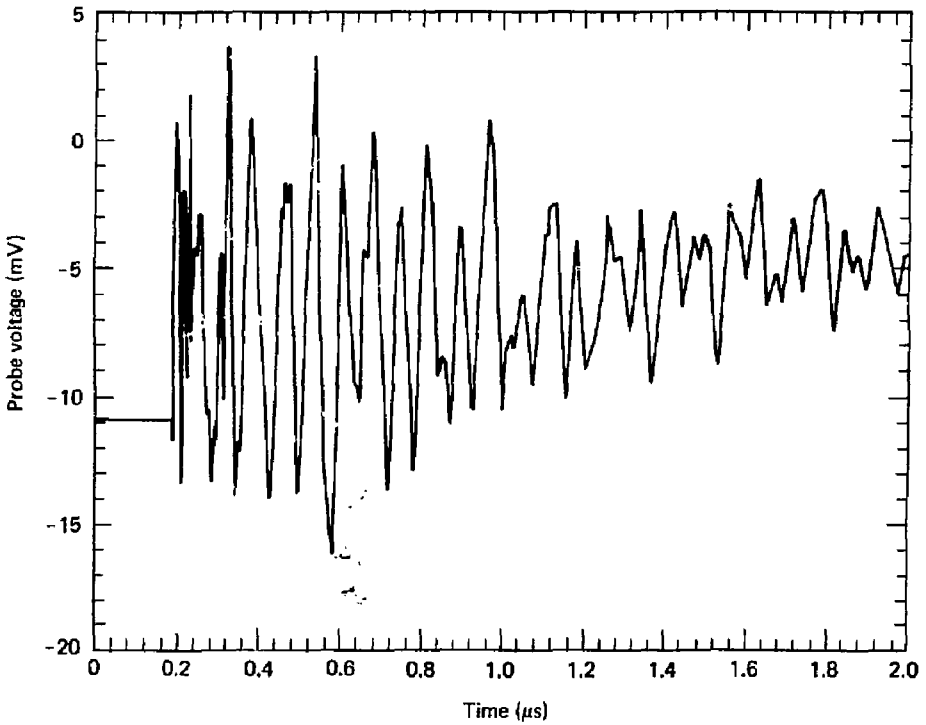

FIGURE 19 Time Domain Plot of Electric Field

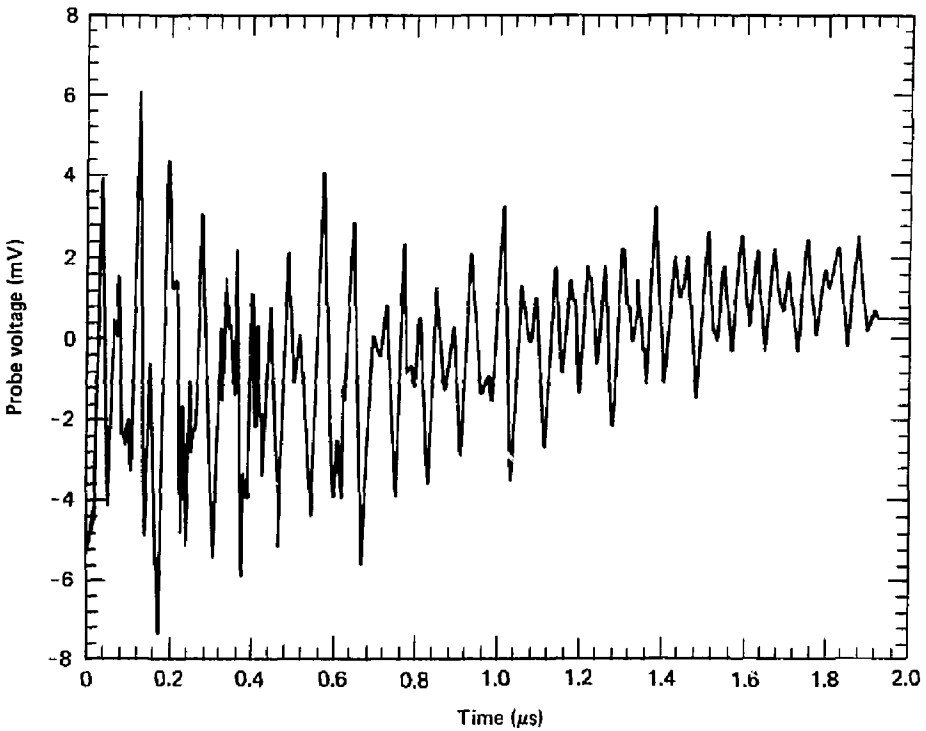

FIGURE 20 Time Domain Plot of Electric Field

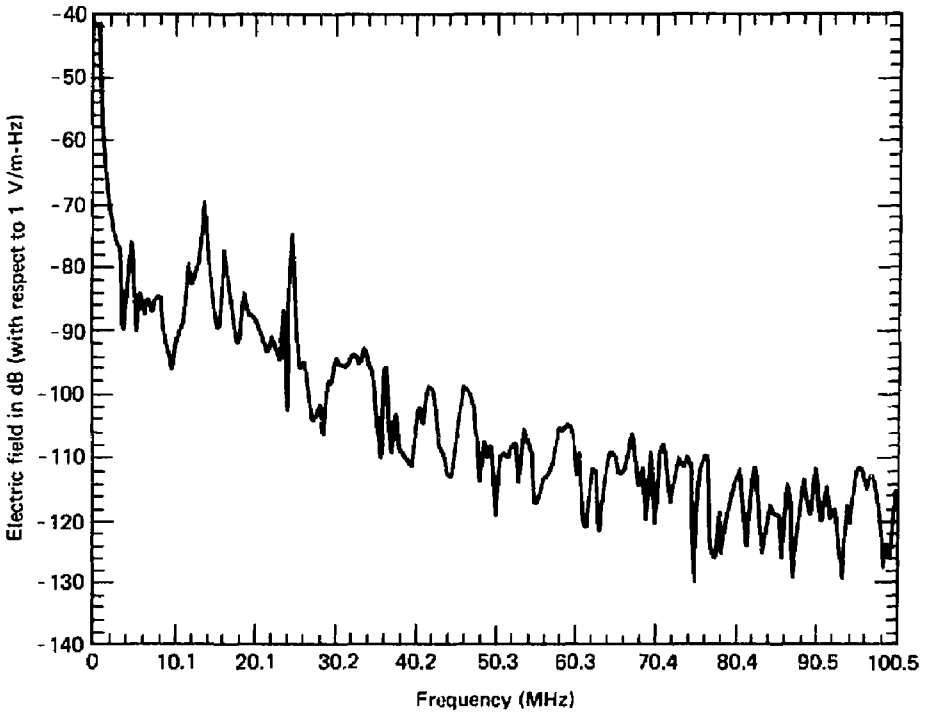

FIGURE 21 Frequency Domain Plot of Electric Field

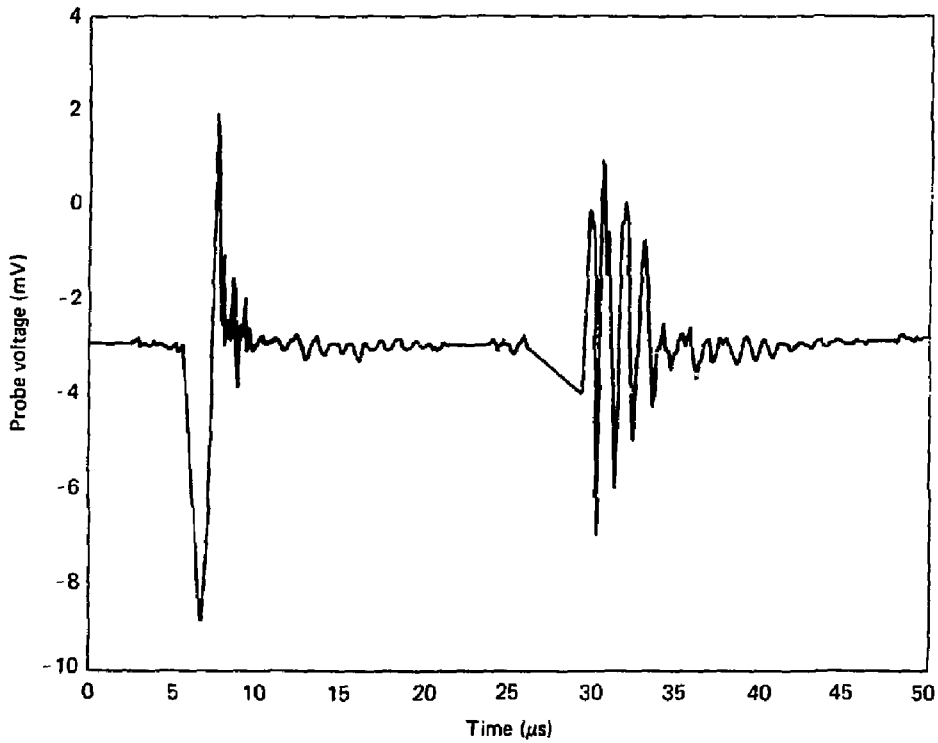

FIGURE 22 Time Domain Plot of Electric Field

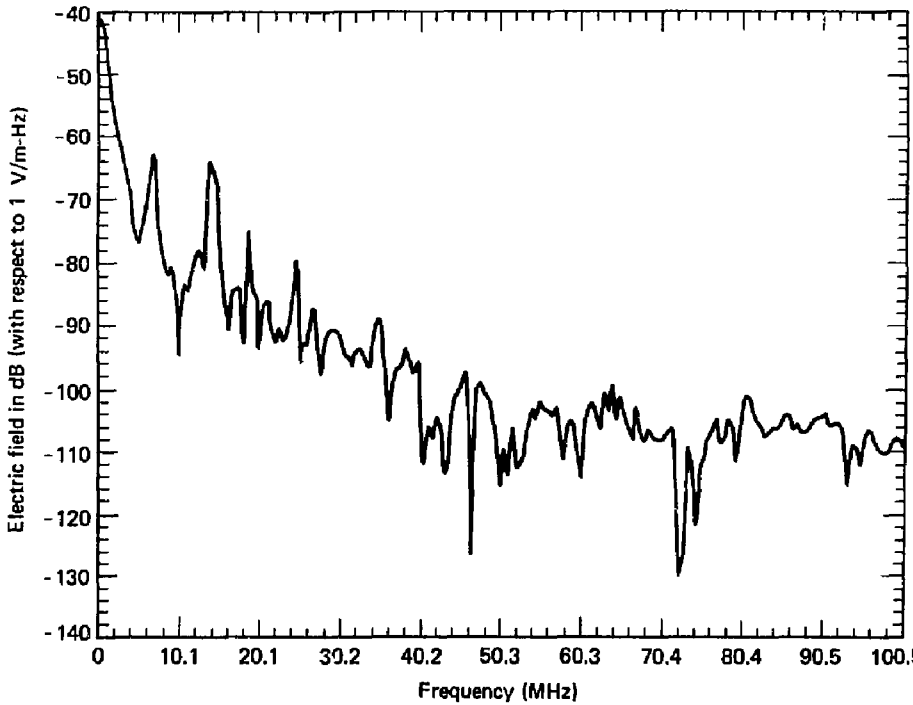

FIGURE 23 Frequency Domain Plot of Electric Field

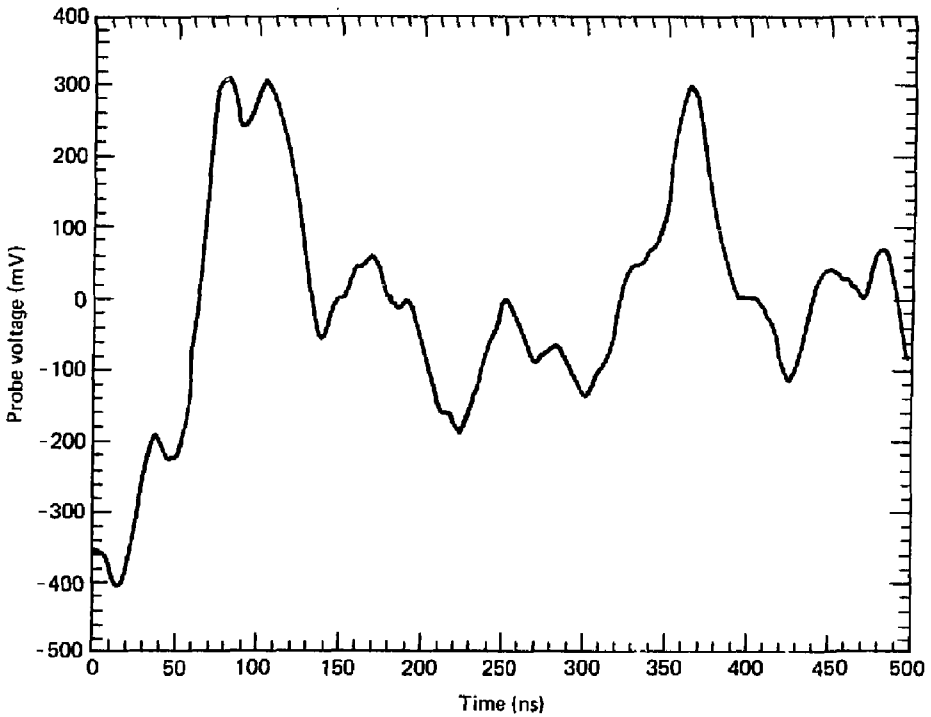

FIGURE 24 Time Domain Plot of Electric Field

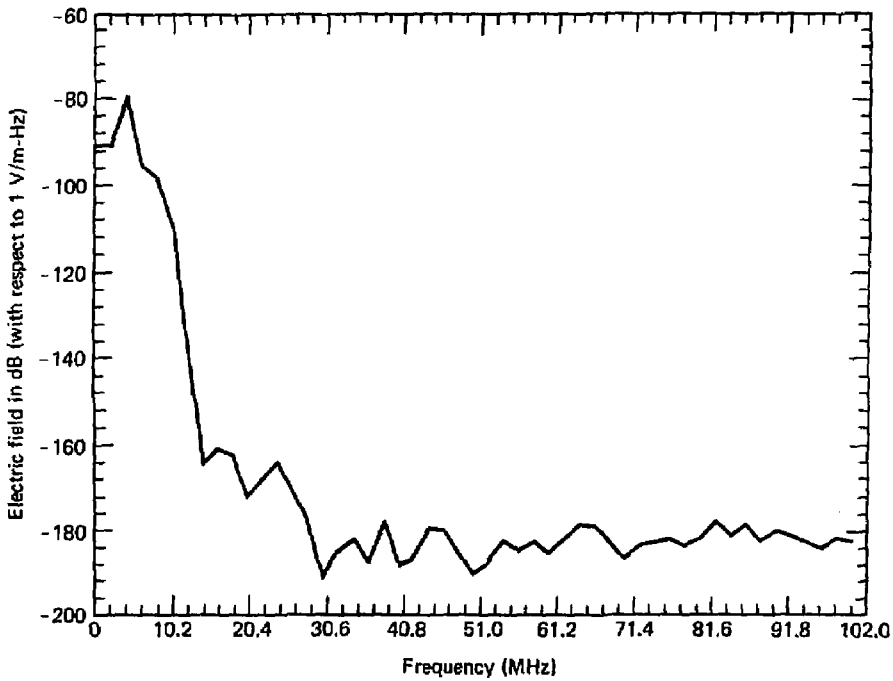

FIGURE 25 Frequency Domain Plot of Electric Field

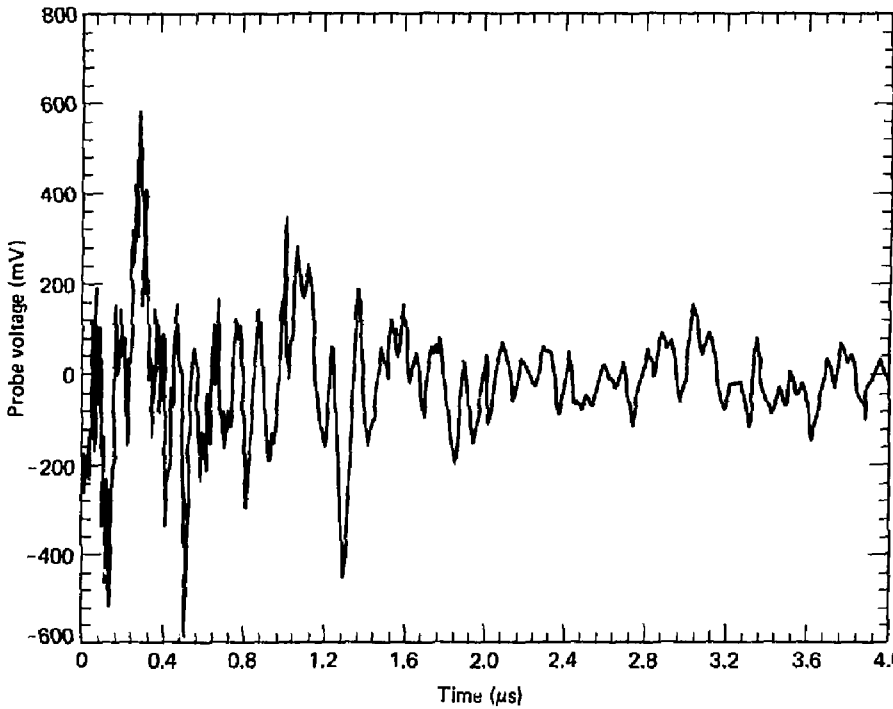

FIGURE 26 Time Domain Plot of Flectric Field

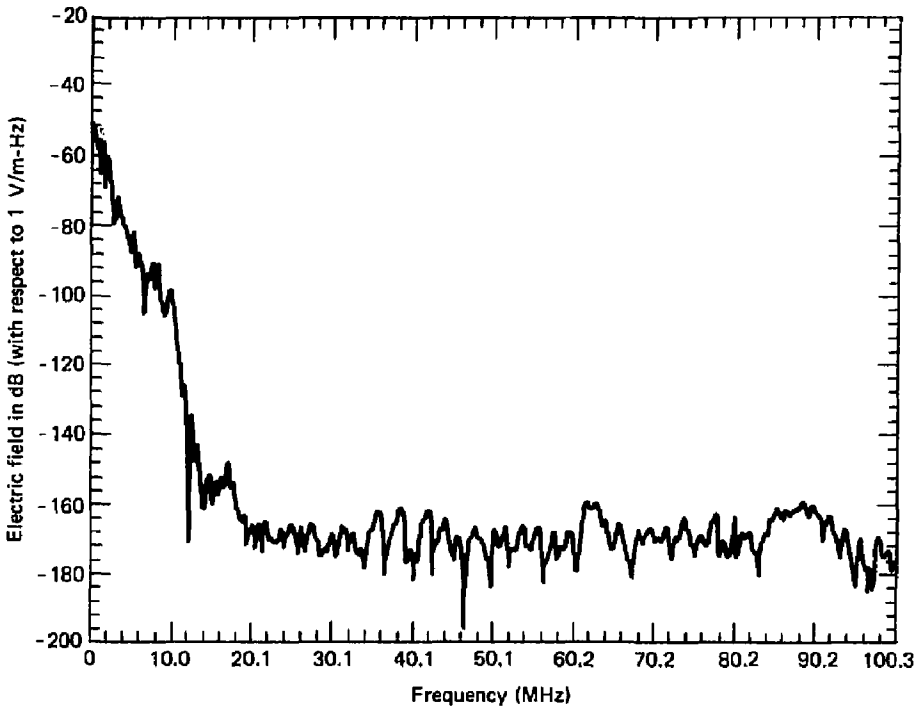

FIGURE 27 Frequency Domain Plot of Electric Field

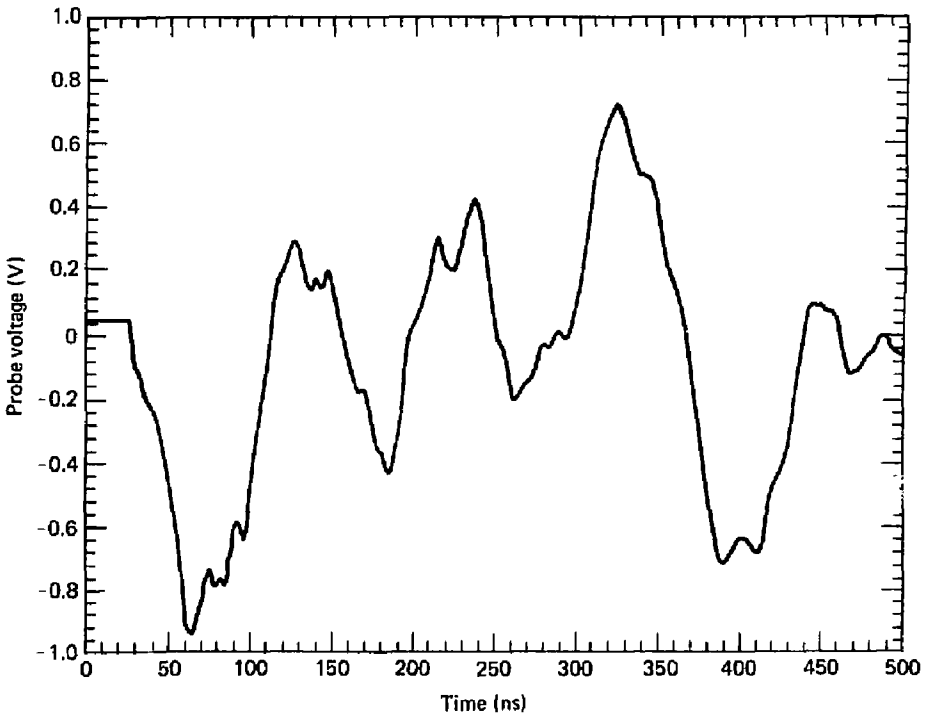

FIGURE 28 Time Domain Plot of Electric Field

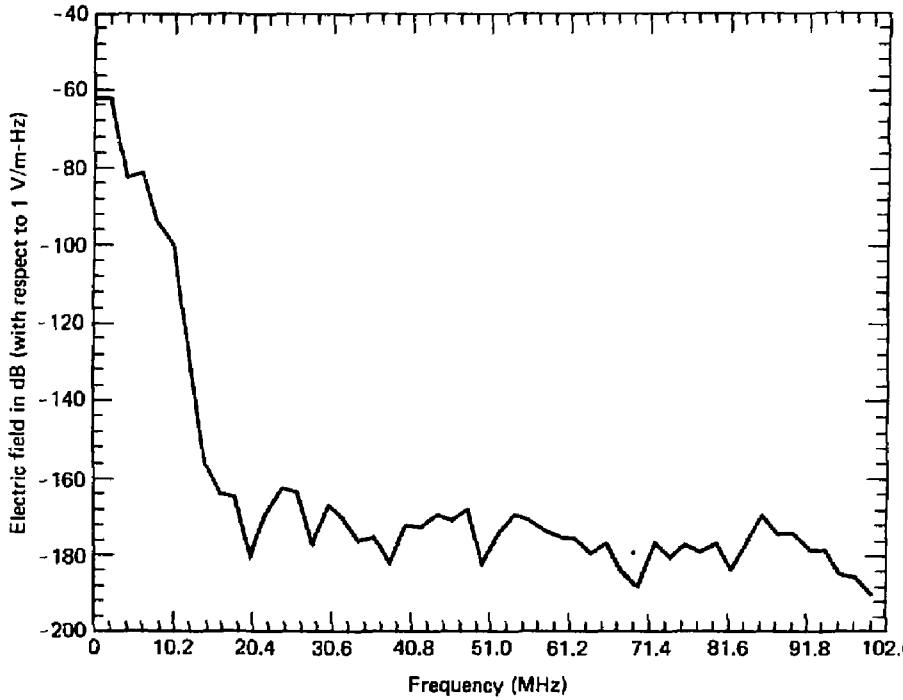

FIGURE 29 Frequency Domain Plot of Electric Field

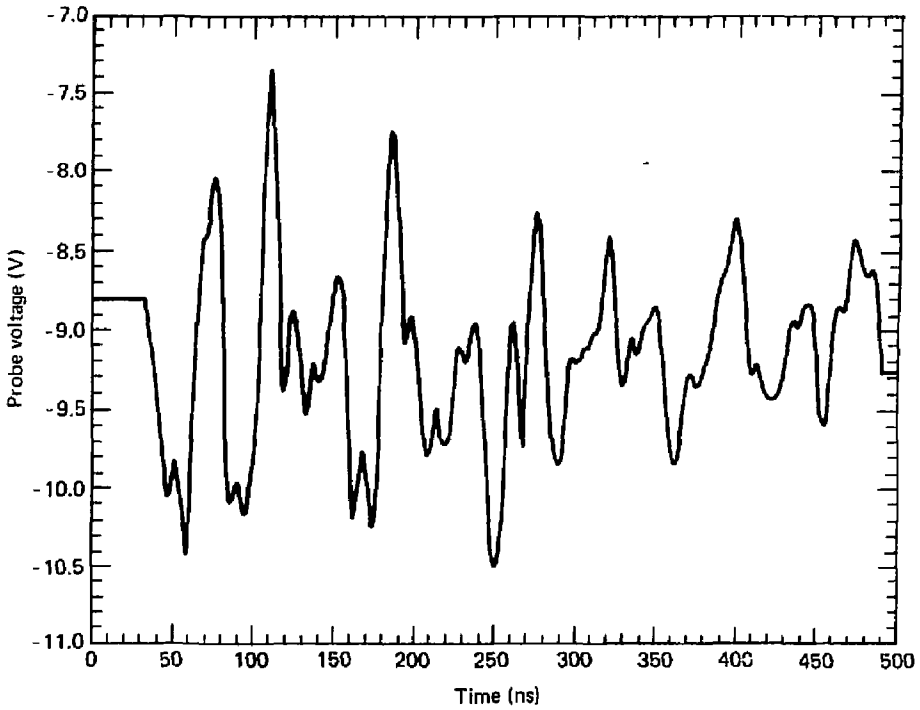

FIGURE 30 Time Domain Plot of Magnetic Field

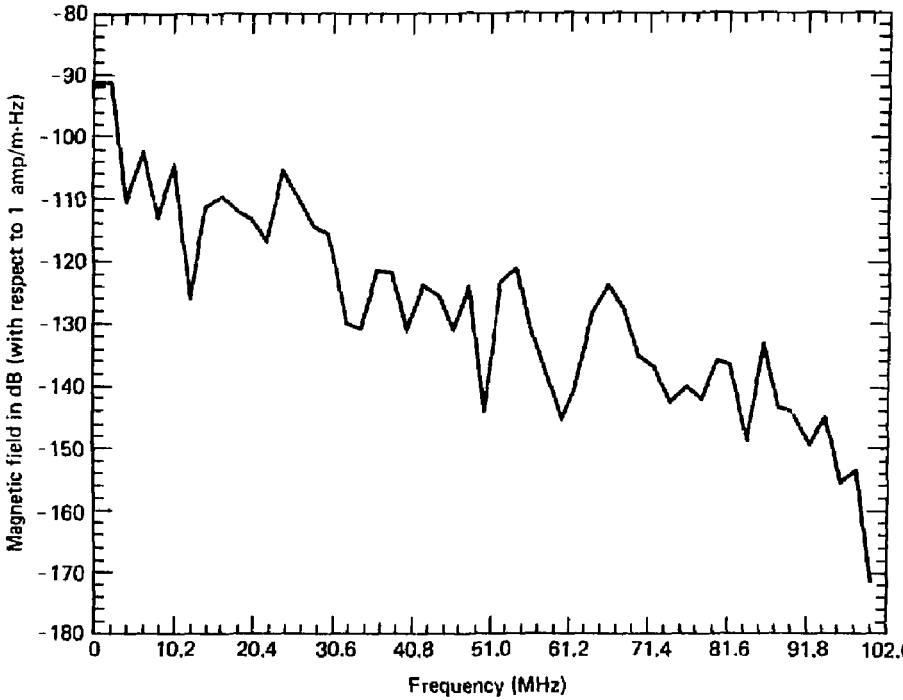

FIGURE 31 Frequency Domain Plot of Magnetic Field

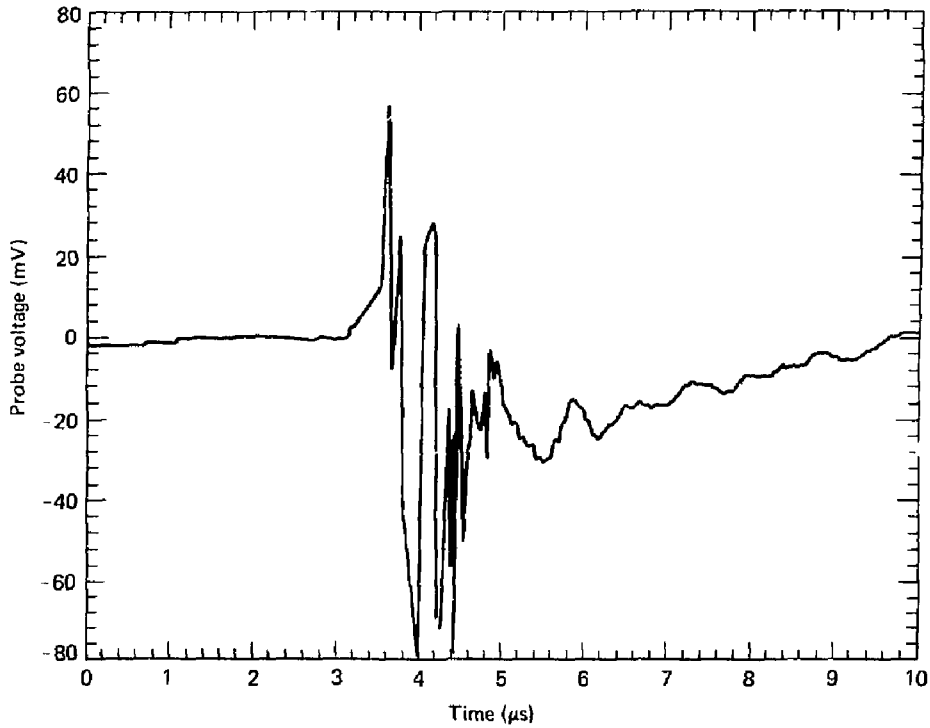

FIGURE 32 Time Domain Plot of Magnetic Field

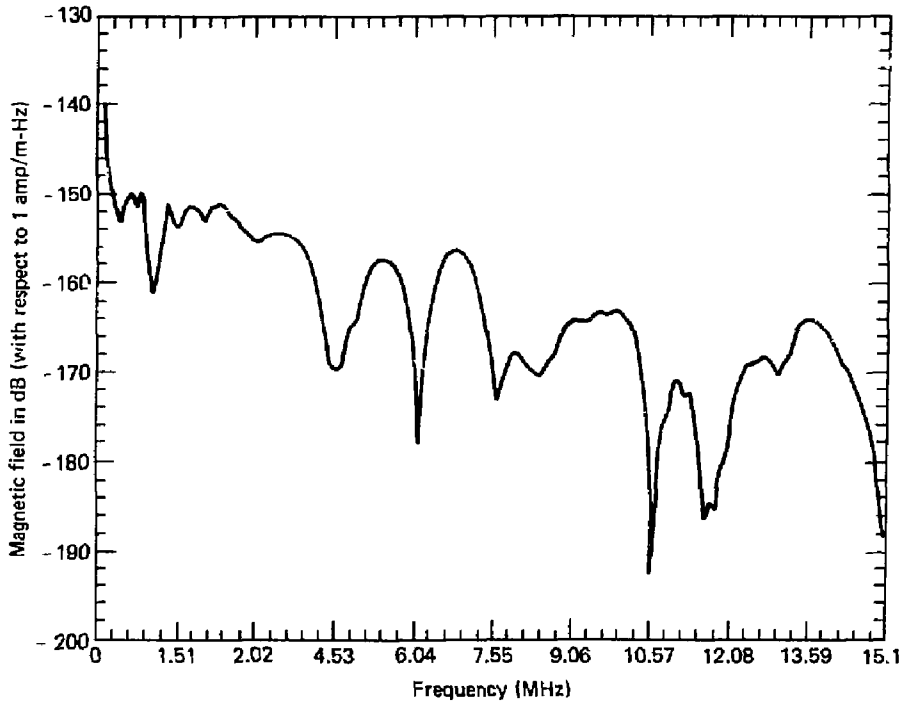

FIGURE 33 Frequency Domain Plot of Magnetic Field

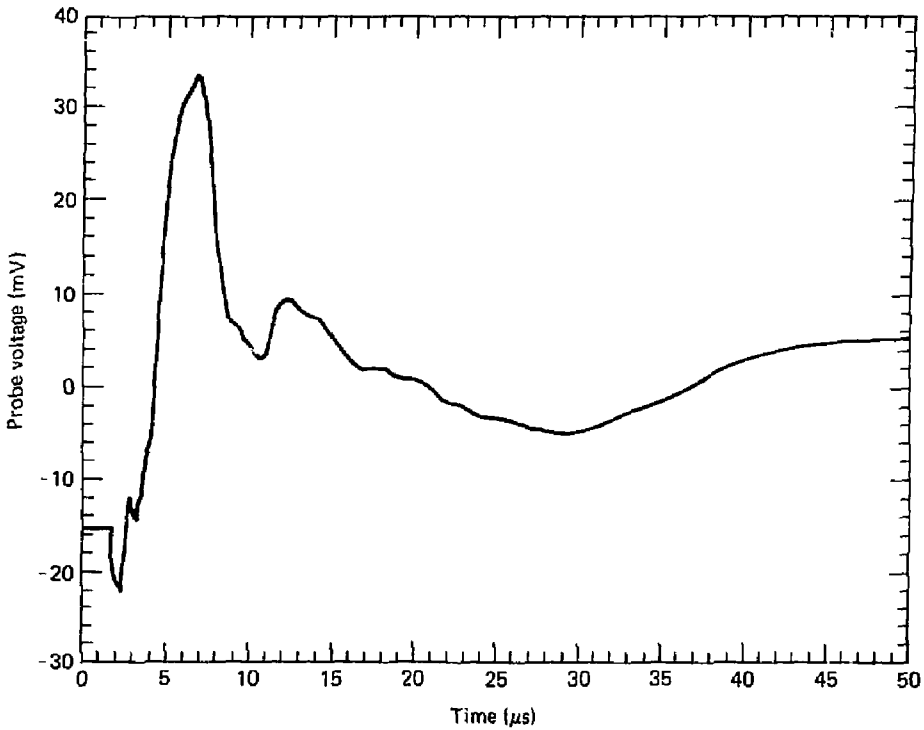

FIGURE 34 Time Domain Plot of Magnetic Field

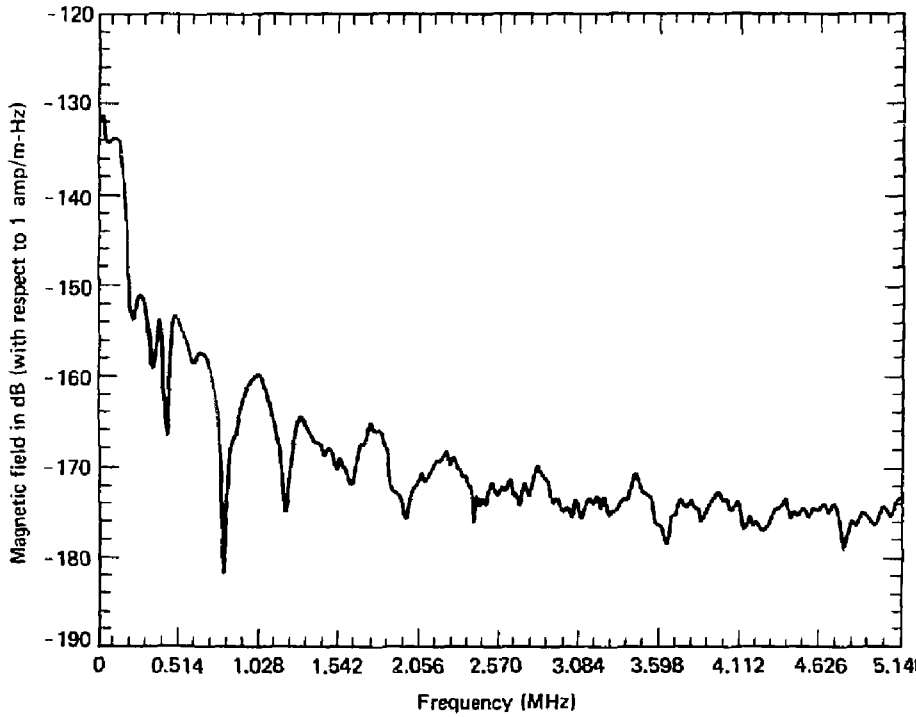

FIGURE 35 Frequency Domain Plot of Magnetic Field

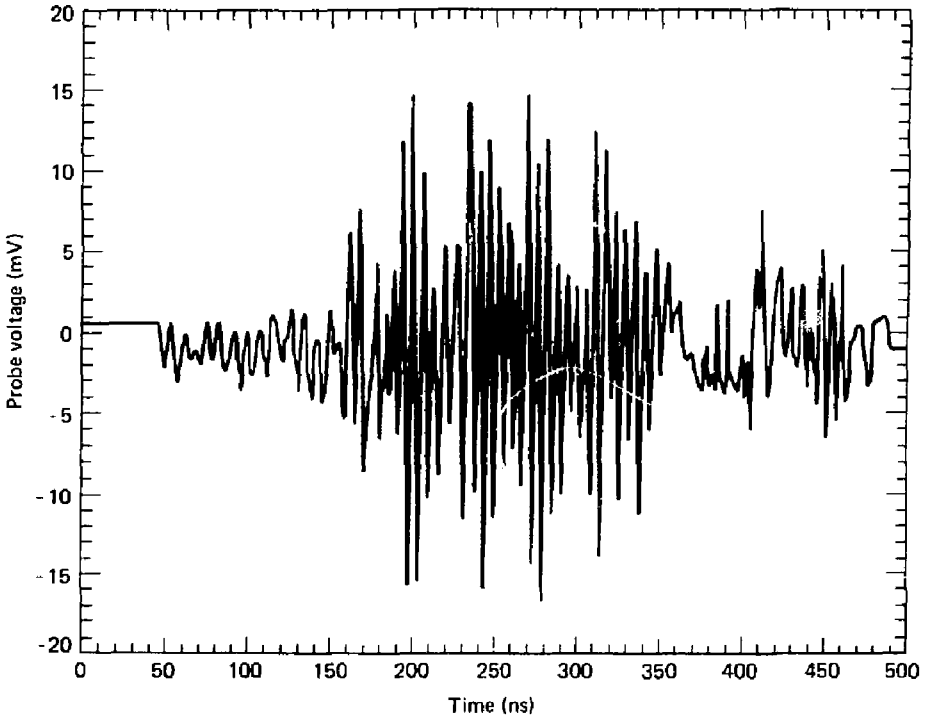

FIGURE 36 Time Domain Plot of Magnetic Field

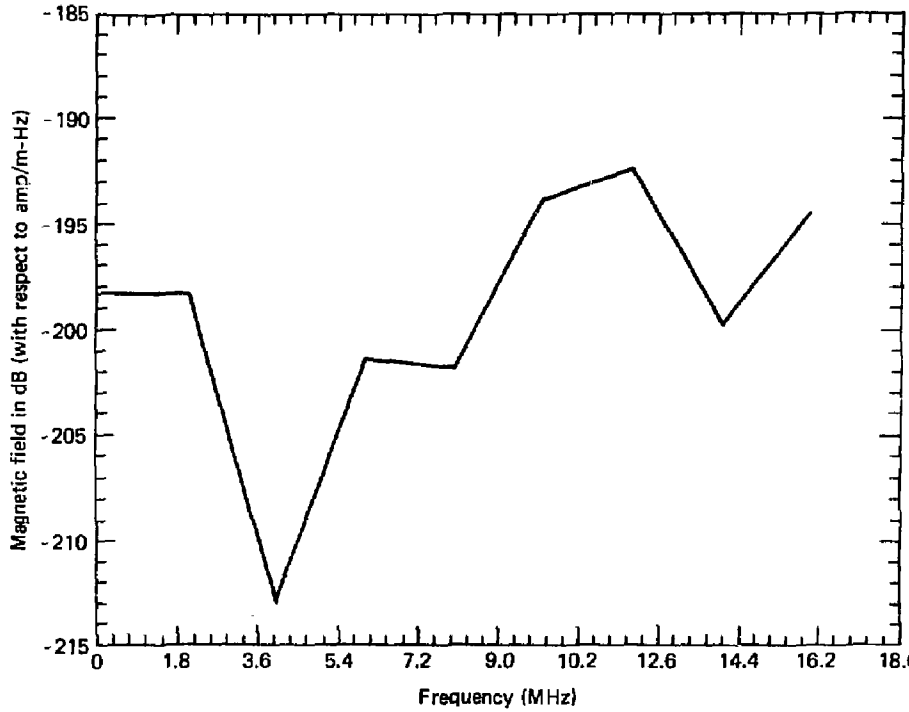

FIGURE 37 Frequency Domain Plot of Magnetic Field

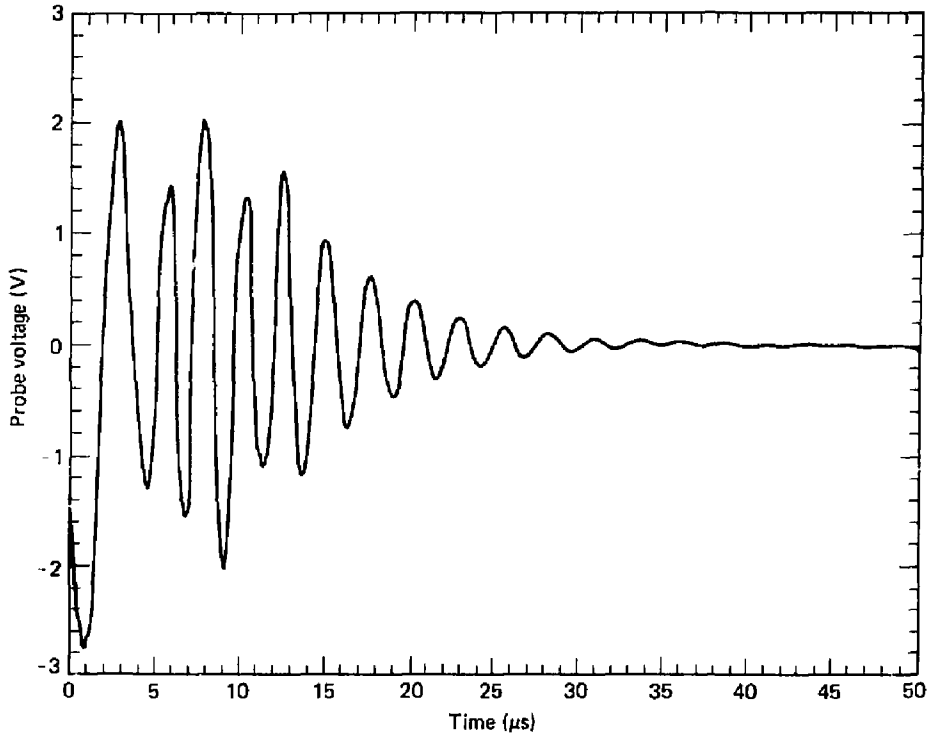

FIGURE 38 Time Domain Plot

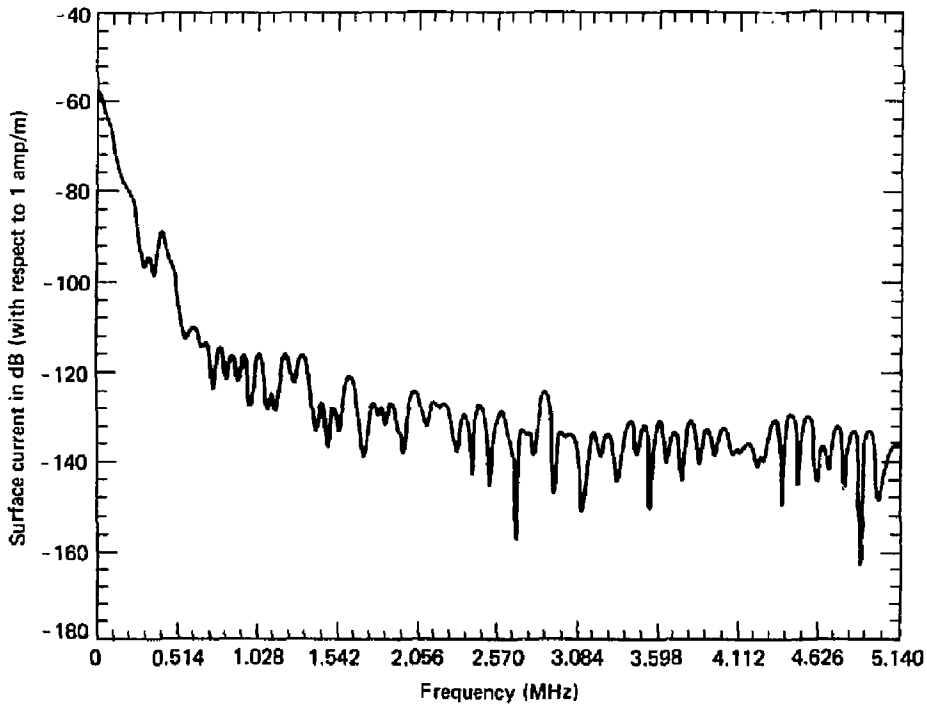

FIGURE 39 Frequency Domain Plot

In Section 2.2, several sources of EM radiation were identified. The charging of the Blumleins and discharging should give rise to frequencies in the few MHz and somewhat above 10 MHz respectively. The spark gaps can generate frequency components in the 10's of MHz (probably around 50). In addition, the ETA will itself re-radiate fields at several resonant frequencies: 6, 9, 15 and 31 MHz. [For details see Appendix A.] The beam itself when fired will generate its own frequencies. The charge trigger occurs about 20 μs before the fire trigger. All records taken using the charge trigger will not record frequencies due to the discharge because the time records are less than 20 μs.

These frequencies are all summarized in Table 3. In addition, possible harmonics are also tabulated for Blumlein charging and discharging. The significant resonances observed in the frequency data for the electric field and magnetic field are shown in Tables 4 and 5 respectively. The amplitudes in dB (with respect to unity with proper units) and probable sources are also shown. The time histories which correspond to probe raw data are included for completeness. They all exhibit very oscillatory nature. Figure 19 is interesting because it shows rather clearly the fields produced when charging and discharging occur. The abbreviations used in Tables 4 and 5 for the probable sources are shown in Table 3. The on, off, charge and fire refer to the beam condition and the trigger setting. The surface currents in Table 5 are all in dB and given in A/m-Hz. They should be multiplied by the circumference to obtain total current A/Hz. The cable current time history recorded with the current probe (Figure 38) yielded frequency data up to 5 MHz. In this range, no significant resonances are observed (Figure 39).

TABLE 3. Expected Resonance Frequencies from ETA and Components

SOURCE	EXPECTED RESONANT FREQUENCY
Blumlein Charging (BC)	few MHz (< 5 MHz)
Blumlein Charging (1st harmonic)	between 5 and 10 MHz
ETA (axial Dimension) (ETA/A)	around 9 MHz
ETA with rails (ETA/R)	around 6 MHz
Blumlein Discharging (BD)	above 10 MHz (10 to 20 MHz)
ETA (Vertical Dimension) (ETA/V)*	around 15 and/or 31 MHz
Blumlein Discharging (1st harmonic)	between 20 and 40 MHz
Spark Gaps (SG)	ten's of MHz (~50 MHz)

*If the ground plane is a good conductor, the ETA will act as a quarter wavelength resonant structure and radiate fields at 15 MHz. Otherwise it will a half-a-wavelength resonant structure and radiate at 31 MHz.

TABLE 4. Electric Field Data (V/m-Hz)

FREQUENCY MHz	AMPLITUDE dB	PROBABLE SOURCE
.Vertical E-Field at Target End (on, fire) (Fig. 18)		
10	-116	ETA/A
14	-116	B.D.
24	-120	B.D.
36	-116	B.D.
53	-113	S.G.
.Normal E-Field at Cathode End (off, fire) (Fig. 21)		
4	-76	ETA/R
13	-70	B.D.
16	-78	B.D.
25	-74	B.D.
34	-92	ETA/V
36	-96	B.D.
42	-100	B.D.
48	-100	S.G.
.Normal E-Field at Cathode End (on, fire) (Fig. 23)		
6	-63	ETA/R
14	-64	B.D.
18	-75	B.D.
25	-80	B.D.
27	-88	B.D.
35	-90	B.D.
.Horizontal E-Field Outside Building (off, fire) (Fig. 25)		
4	-80	ETA/R
16	-160	B.D.
24	-163	B.D.
33	-182	B.D.
37	-180	B.D.
45	-180	B.D.
64	-180	?
84	-180	?
.Horizontal E-Field Outside Building (on, charge) (Fig. 27)		
3	-52	B.C.
13	-136	?
18	-148	?
36	-160	?
39	-160	?
42	-160	?
62	-160	?
88	-160	?

TABLE 4. Electric Field Data (V/m-Hz), (Continued)

FREQUENCY MHz	AMPLITUDE Db	AMPLITUDE SOURCE
.Horizontal E-Field Outside Building (on, fire) (Fig. 29)		
24	-164	B.D.
31	-168	ETA/V
46	-168	B.D.
53	-168	S.G.
84	-168	?

TABLE 5. Magnetic Field and Surface Current Data (A/m-Hz)

FREQUENCY MHz	AMPLITUDE Db	PROBABLE SOURCE
.Axial Current at Cathode End (on, fire) (Fig. 31)		
6	-104	ETA/R
10	-106	ETA/A
16	-110	B.D.
24	-106	B.D.
37	-120	B.D.
42	-124	B.D.
48	-124	B.D.
53	-120	S.G.
65	-124	?
81	-134	?
86	-132	?
.Magnetic Field Inside Building (off, charge) (Fig. 33)		
5.4	-157	B.C.
6.5	-156	ETA/R
9.5	-164	ETA/A
11.0	-171	ETA/A
13.6	-164	ETA/A
.Magnetic Field Inside Building (off, charge) (Fig. 35)		
.5	-154	B.C.
1.0	-160	B.C.
1.25	-165	B.C.
1.7	-165	B.C.
.Magnetic Field Outside Building (on, fire) (Fig. 37)		
10 MHz	-192	ETA/A

6.0 DATA ANALYSIS

6.1 Resonant Frequencies

The field data from the ETA is highly oscillatory as attested to by the number of significant resonances listed in Tables 4 and 5. In Figure 40, these frequencies are shown in histogram form, where the number of occurences within a certain frequency band are plotted. There is a large concentration below 6 MHz (~18%). These resonances are probably due to Blumlein charging. Between 10 and 18 MHz, about 25% of the resonances occur. These are due to ETA resonances and Blumlein discharging. Other resonances between 24 and 40 MHz (about 33%) probably occur due to higher order harmonics from Blumlein discharging. Resonances around 50 MHz (~11%) could be attributed to the spark gaps. The concentrations of resonances above 60 MHz (62 to 65 MHz and 81 to 88 MHz) cannot be easily explained. They may be due to even higher harmonics from the Blumleins. These frequencies cannot be attributed to the electron beam itself since they seem to occur when the beam is off or when the charge trigger is used. It should be pointed out that the choice of significant resonant frequencies from the Fourier transform plots is prone to some error. It would be far more superior to apply pole and zero data analysis techniques to the time data. This technique would allow the extraction of the complex resonant poles for the damped time histories and avoid judgmental factors in the choice of significant resonances. Several additional observations can be made.

1 - There are differences in the pattern of resonant frequencies when the beam is off versus on. However, the data is not consistent enough to claim that the differences are due to the beam. A more sophisticated data analysis techniques will be needed for making such assertions.

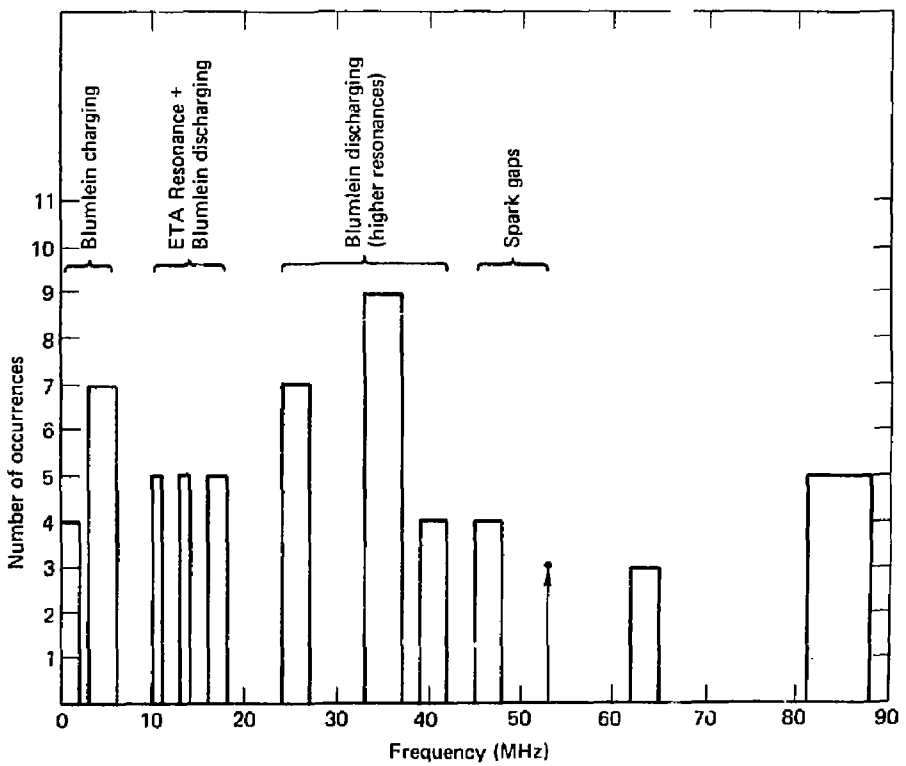

FIGURE 40 Histogram of Resonant Frequency Occurrences

2 - In Table 4, resonances above 60 MHz are detected only with the LP antenna. However, these resonances are also detected with the magnetic field probe at the cathode end. This rules out outside non-ETA sources for these frequencies.

6.2 Field Amplitudes

It will be very difficult to correlate conclusively the field levels from the various shots since the operation level of the ETA was not steady during the time when the data was taken. For example, definitive statements cannot be made about changes in field levels going from inside the building to the outside or for changes due to the mode of operation of the ETA. From the data, upper bounds can be established for fields. Upper bounds for the horizontal electric field outside the building are shown at significant resonant frequencies in Table 6.

The magnetic field data extends to 15 MHz and is only available at the time of writing of this report inside the building at several frequencies. The levels listed in Table 5 should be corrected because no attempt was made to maximize probe reading by proper positioning of the loop antenna. The loop response peaks when the magnetic field vector is prependicular to its surface. At any other angle θ the response is reduced by a factor $f = \cos \theta$. For magnetic fields that are azimuthal with respect to the axis of the ETA, f can be estimated since the loop position with respect to the ETA is known. For the loop inside the building, f = .087. The loop readings therefore should be divided by the reciprocal of this factor. This correction factor is valid only for azimuthal magnetic fields with respect to the ETA axis. In Table 7, the magnetic field amplitudes are tabulated with and without this correction factor.

TABLE 6. Peak Amplitudes of Horizontal Electric Field Outside ETA Building

Frequency (MHz)	Amplitude(V/m-Hz)
3	2.5×10^{-3}
13	1.6×10^{-7}
18	$4. \times 10^{-8}$
36	$1. \times 10^{-8}$
39	$1. \times 10^{-8}$
42	$1. \times 10^{-8}$
62	$1. \times 10^{-8}$
88	$1. \times 10^{-8}$

TABLE 7. Peak Amplitudes of Magnetic Fields Inside ETA Building

Frequency (MHz)	Amplitude (A/m-Hz) Loop Reading	Amplitude (A/m-Hz) With Correction Factor
.5	$2. \times 10^{-8}$	2.3×10^{-7}
1.	$1. \times 10^{-8}$	1.14×10^{-7}
1.25	5.6×10^{-9}	6.4×10^{-8}
1.7	5.6×10^{-9}	6.4×10^{-8}
5.4	1.4×10^{-8}	1.6×10^{-7}
6.5	1.6×10^{-8}	1.8×10^{-7}
9.5	6.3×10^{-9}	7.2×10^{-8}
11	2.8×10^{-9}	3.2×10^{-8}
13.6	6.3×10^{-9}	7.2×10^{-8}

The only loop reading outside the building is at 10 MHz. Without correction this yields a peak amplitude = 2.5×10^{-10} A/m-Hz, and with correction, peak amplitude = 7.6×10^{-9} A/m-Hz. From Table 6, the peak electric field closest to 10 MHz is 1.6×10^{-7} V/m-Hz. The ratio of peak electric field to peak corrected magnetic field is 21 Ω, and for the peak uncorrected field it is 640. For radiated fields, this ratio is 377 Ω. For near-fields, it is much smaller. The ratio for the corrected magnetic field is therefore in the right range.

In Appendix A, the ratio of current to radial electric field at the tip of a cylinder approximating the ETA was shown to be $I/E = 1.15 \times 10^{-3}$ A/V/m at resonance. The axial surface current values in Table 5 at the cathode end should be multiplied by the cathode circumference to obtain the total current (circumference = .74 m). At about 10 MHz, $I = 3.7 \times 10^{-6}$ A/Hz and $E = 3.16 \times 10^{-4}$ V/m-Hz. The ratio $I/E = 11.7 \times 10^{-3}$. This is an order of magnitude larger than the expected ratio and most probably due to shot-to-shot variations in the ETA.

Also in Appendix A, the ratio of the current at the midpoint to the current at the tip was found to be 5.7. This predicts a current at the middle $I = 21 \times 10^{-6}$ A/Hz (at resonance). This current sets magnetic fields $H = I/2\pi r$ (r is the radius away from the axis). For the loop position inside the building, $H_i = 5.5 \times 10^{-7}$ A/m which is an order of magnitude larger than the peak corrected amplitude in Table 7. The predicted value outside the building is larger than the corrected loop reading by a factor of = 27. This is probably due to shot-to-shot variations and also to the shielding provided by the building. In Table 4, the vertical electric field amplitudes at the target end

are significantly lower than those at the cathode end. At the cathode end the probe is surrounded by several cables from the grid pulse circuit. This really suggests that there is really more noise at the cathode end.

7.0 CONCLUSIONS

The electromagnetic fields in the immediate vicinity of the ETA have been measured. The frequency content has been displayed up to 100 MHz. Significant concentrations of resonant frequencies from the various probe readings have been observed. Attempts have been made to correlate the amplitudes of the fields from the various. The following observations can be made.

- The frequency coverage provided by the several probes is adequate. The capability extends into the low GHz region. Information up to 100 MHz has been displayed in this report.

- The amplitude readings from the various probes are consistent to within an order of magnitude. This is mostly due to shot-to-shot variations of the ETA, the very approximate analytical techniques used to model the ETA in an electromagnetic sense, and also due to unknowns such as building shielding and rebar structure.

- The Fourier transform techniques used to analyze the data is not quite adequate. Improved data processing techniques can simplify the process of choosing the significant resonant frequencies.

- In most cases, the probable sources of the resonances observed could be identified. However, some cases have no obvious explanation. The ETA is a highly complex machine and as the power conditioning diagrams show in Figure 2, it is a source of many resonant frequencies and higher harmonics which cannot be uniquely identified.

- The available data was not conclusive enough as far as identifying changes in the fields both in amplitude and frequency due to the beam itself.

Recommendations for future improvements in this area include:

- Use of the poles representation of the damped signals from the ETA to better identify the resonant frequencies and their relative significance. This might provide a better alternative to identifying the various components of the ETA as far as their contributions to the frequency spectrum.

- It will be very useful to monitor the actual charge, discharge and electron beam waveshapes while the fields are being recorded. These can then be analyzed for their frequency content to establish a one-to-one correspondence with the field data.

- It will be useful to do simultaneous electric and magnetic field measurements in order to better correlate their amplitudes.

- A current injection test of the ETA can be very useful in terms of identifying all the structural resonances.

REFERENCES

1) R. Hester, D. Bubp, J. Clark, A Chesterman, E. Cook, W. Dexter, T. Fessenden, L. Reginato, T. Yokota, A. Faltens, "The Experimental Test Accelerator (ETA)," 1979 Particle Accelerator Conference, March 12-14, 1979 (also UCRL-82448).

2) W. Barletta, "Accelerating Intense Electron Beams," UCRL-52000-79-9.

3) D. Rodgers, W. Dexter, A. Myers, L. Reginato, A. Zimmerman, "Modulator Charging System Upgrade for a 5 MeV Electron Accelerator," IEEE 1978 Thirteenth Pulse Power Modulator Symposium.

4) E. Cook, L. Reginato, "Off Resonance Transformer Charging for 250-kV Water Blumlein," IEEE 1978 Thirteenth Pulse Power Modulator Symposium.

5) A. Faltens, L. Reginato R. Hester, E. Cook, A. Chesterman, T. Yokota, W. Dexter, "High-Repetition-Rate Burst-Mode Spark Gap," IEEE Thirteenth Pulse Power Modulator Symposium.

APPENDIX A

ETA EM Description

In this Appendix, the ETA metallic structure will be discussed with the objective of predicting approximately its radiating characteristics including the resonances. In addition, sensor locations with respect to the ETA will be sketched.

In Figure A1, a sketch of the ETA (side view) is presented. A picture is shown in Figure A2. The complexity of the structure is such that predicting its radiating properties will be extremely difficult. Only rough estimates can be made here. It can be observed in Figure A1 that the ETA is a rather massive metallic object 54 feet long resting on steel rails that make the whole metal structure 84 feet long. The entire ETA rests on concrete which is reinforced with rebar. The height of the ETA from the floor to the top of the Blumleins is about 16 feet and the width is about 12 feet. A 54-foot cylinder (assuming a cylinder is electrically a good approximation to the ETA) with axial currents induced on it resonates at about 9 MHz. With the rails, which make the structure 84 feet long, the resonance occurs at about 6 MHz. Even though the ETA is metallically connected to the rails, these two distinct resonances should be observable. In this discussion, the mutual coupling between ETA (including the rails) and the metal rebar in the floor walls and ceilings is being neglected. (The coupling with the metal door shown at the left in Figure A1 is also being neglected.) Attempts at including these effects will require large amounts of computer modeling. Aximuthal currents flowing from the Blumleins down to the rails may themselves resonate at about 31 MHz. If the ground plane acts as good conductor, this resonance would occur at 15 MHz.

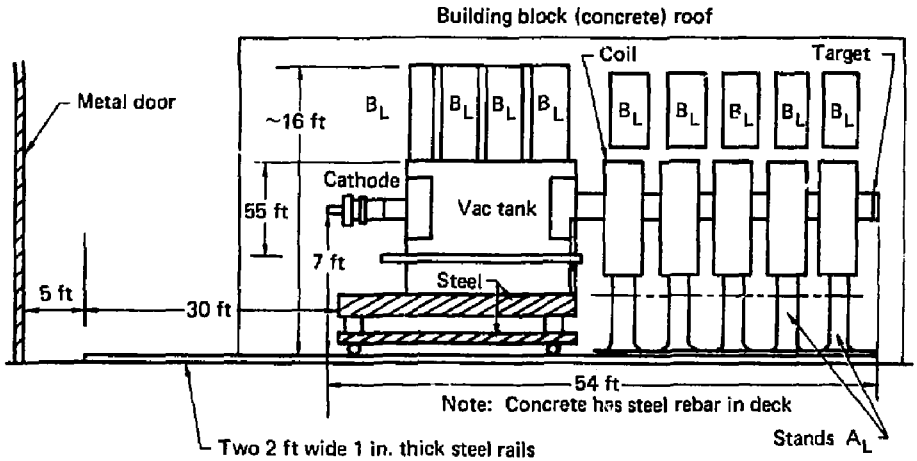

FIGURE A1 ETA Sketch (Side View)

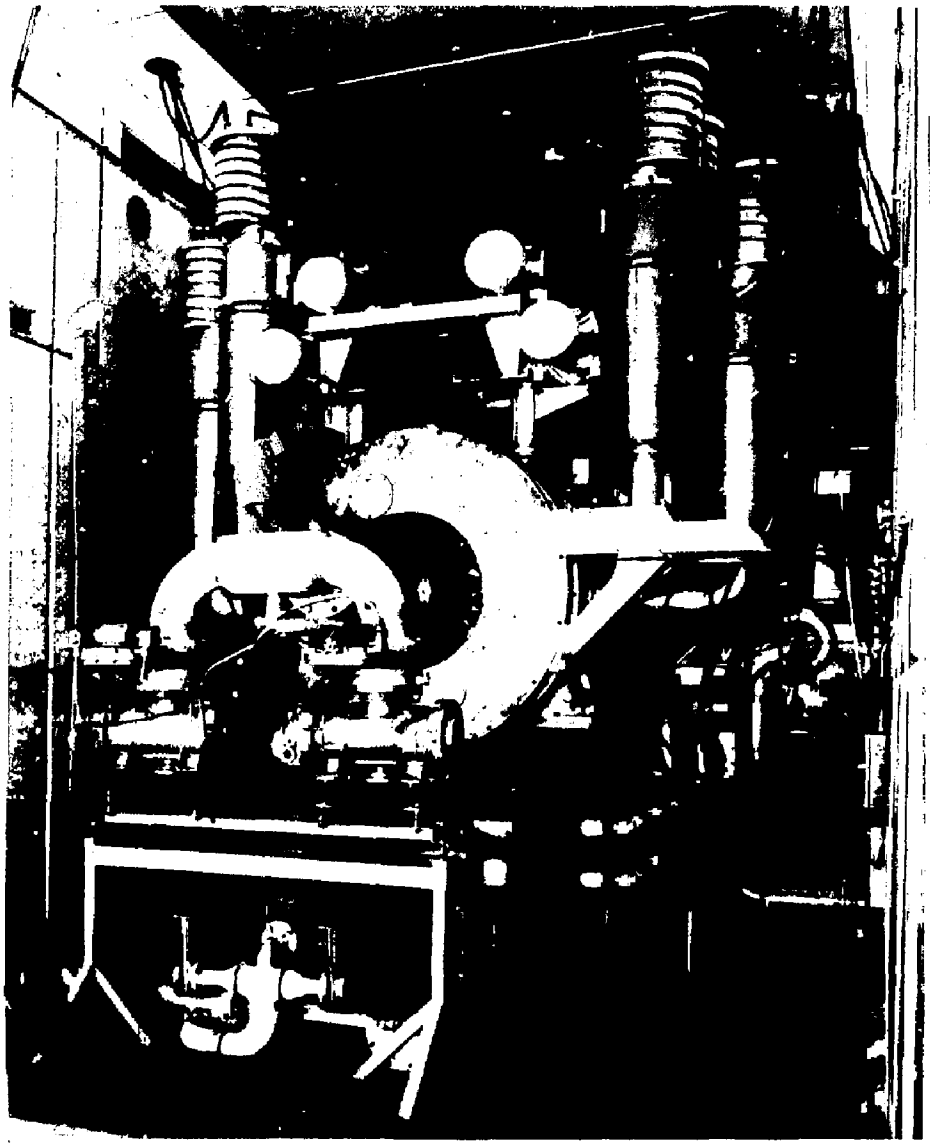

Figure A2. View of ETA

The fatness factor Ω of a cylinder is a measure of its Q value at resonance. It is defined as

$$\Omega = 2 \ln \frac{L}{a}$$

where L is the length and a the radius. For the ETA, this fatness factor is somewhere between 3.8 and 4.4 depending on whether half the height or half the width is used for a value of the radius [the length used is 54 feet]. The Ω is important because the radiating properties of a cylinder are dependent on it. In Figures A3 and A4, the normalized induced axial current and radial electric fields on cylinder (Ω = 6) are shown as a function of frequency for a plane wave incident field. [These figures are taken from Ref. 1.] These relate the currents and normal electric fields at various locations along the cylinder. For the ETA, the Ω is smaller than 6 but these curves are still useful since the variations with Ω are almost linear and in the same proportion of the current and the electric field. For example, at the tip of the 54 foot cylinder the ratio of current to normal electric field is

$$I/Er = 1.15 \text{ mA/(V/m)}$$

In addition, the ratio of the current at the center of the cylinder to that at the tip is about 5.7. These expressions will be useful for interpreting some of the probe data.

References:

1 - "Electromagnetic Pulse Handbook for Missiles and Aircraft in Flight," Sandia Laboratories, SC-M-71.0346, September 1972.

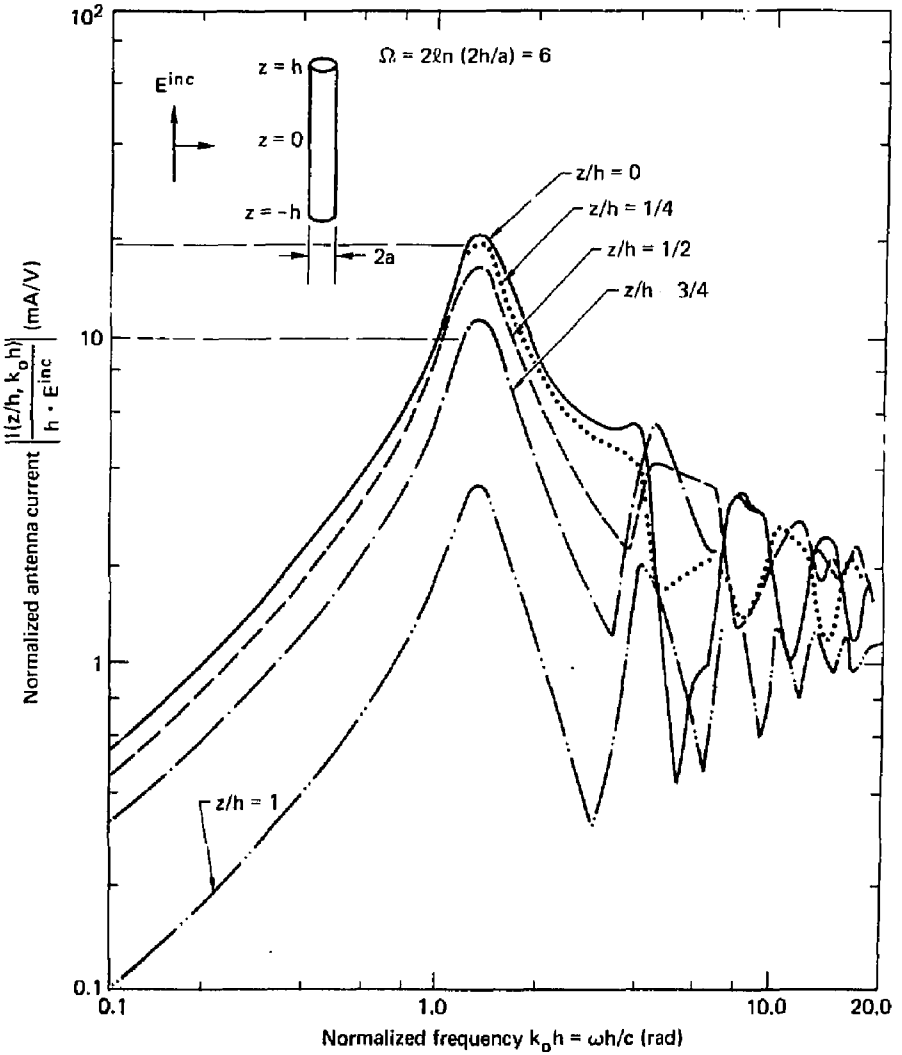

FIGURE A3 Transfer Function for Total Axial Current on a Cylinder with Endcaps

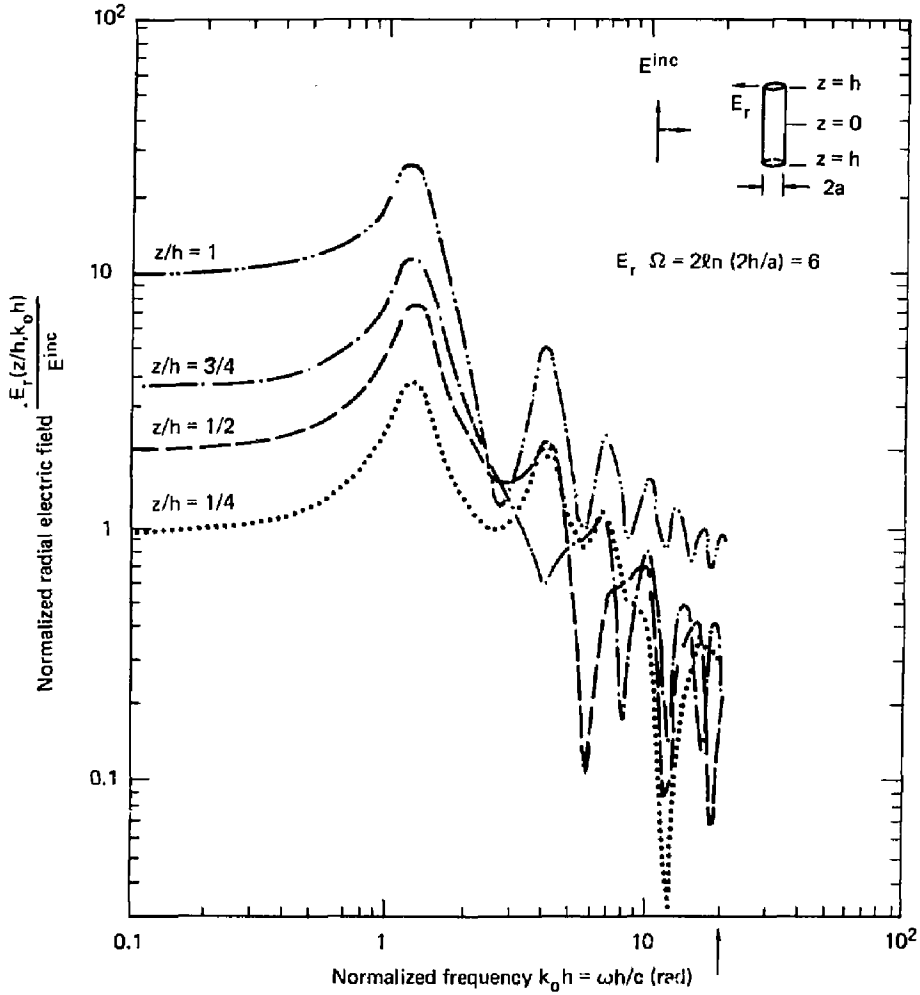

FIGURE A4 Normalized Radial Electric Field at the Surface of the Cylinder with Endcaps

APPENDIX B

Computer Model of 30-Element Log-Periodic Antenna

A computer model was developed for the 30-element log-periodic antenna (model AEL-APN-1509) to determine the low frequency response of this antenna when it is used in measuring field strength. The antenna was modeled with the Numerical Electromagnetics Code (NEC) (Ref. 1) which uses the method of moments to solve the electric field integral equation for current induced on the antenna. In this solution, the antenna elements are represented by strings of short segments. The current on each wire is represented as a sum of smooth basis functions of unknown amplitude, and the electric field boundary condition is enforced at the center of each segment. This leads to a matrix equation to be solved for the basis function amplitudes which determine the current. Options in NEC that were used in this model include R-L-C loads on wires and use of the ideal transmission line equations rather than the integral equation method for modeling transmission lines.

A schematic diagram of the antenna model is shown in Figure B1 while the element dimensions and values of the inductances are given in Tables B1 and B2. Although some of the smaller elements are not exactly aligned on opposite sides of the transmission line they were aligned in the model for convenience. In the actual antenna the transmission line consists of two aluminum rods of square cross section 1 1/2 inches on a side with 1 inch separation at the inside surfaces and terminated in a short circuit. The characteristic impedance of the line was estimated to be 71 ohms. The values of inductances on elements 23 through 30 were estimated from the coil dimensions and number of turns.

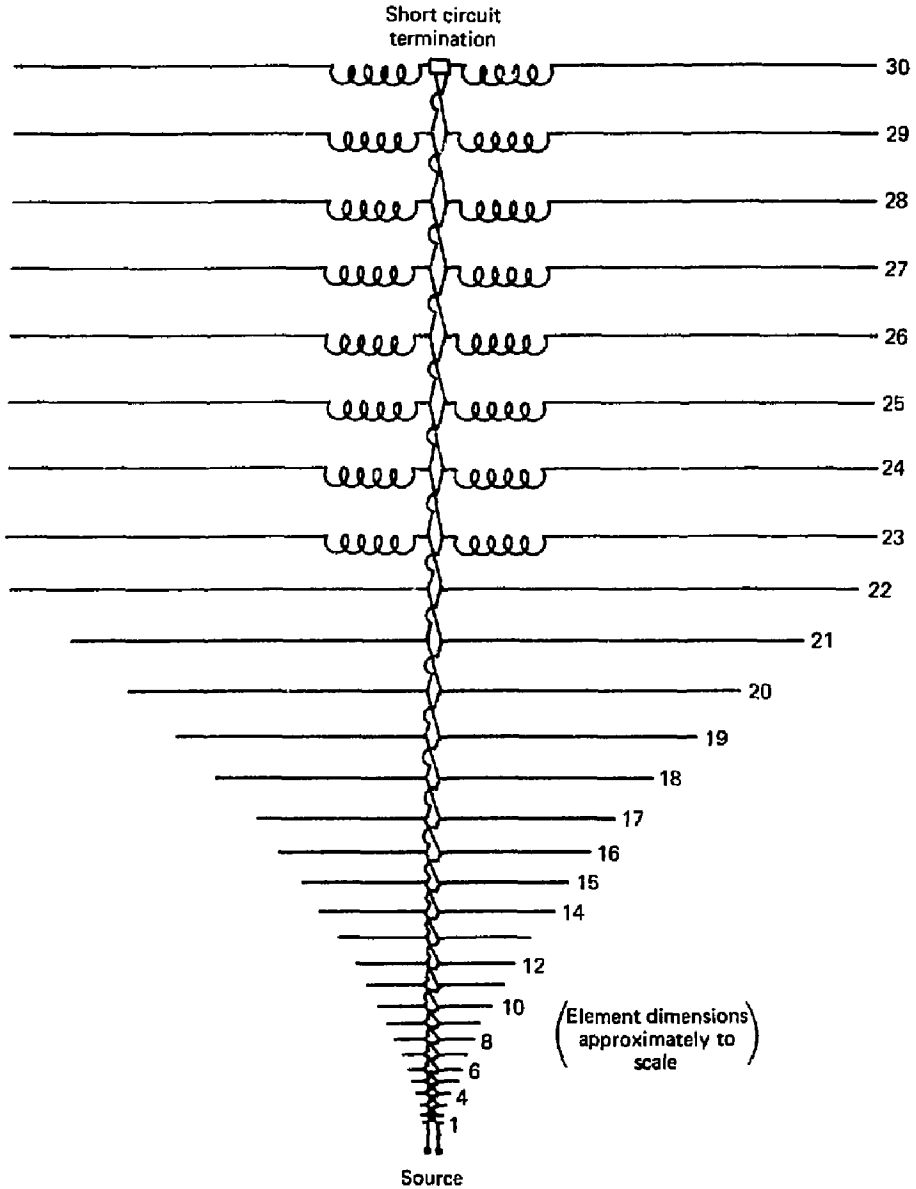

FIGURE B1 Schematic Diagram of Model for 30-Element Log-Periodic Antenna (AEL-APN-1509)

TABLE B1. Antenna Element Dimensions (lengths in meters)

ELEMENT	HALF-LENGTH	POSITION ALONG TRANSMISSION LINE	RADIUS
1	0.0444	0.4260	6.35×10^{-3}
2	0.0572	0.4664	"
3	0.0698	0.5107	"
4	0.0826	0.5593	"
5	0.1016	0.6124	"
6	0.1238	0.6706	"
7	0.1524	0.7343	"
8	0.1778	0.8040	"
9	0.2159	0.8804	7.937×10^{-3}
10	0.2540	0.9640	"
11	0.3048	1.056	"
12	0.3619	1.156	"
13	0.4286	1.266	"
14	0.5461	1.386	"
15	0.5969	1.518	"
16	0.7017	1.662	"
17	0.8033	1.820	"
18	0.9811	1.993	"
19	1.168	2.182	"
20	1.378	2.389	"
21	1.641	2.616	"
22	1.911	2.865	"
23	1.962	3.094	"
24	1.962	3.399	"
25	1.962	3.704	"
26	1.962	4.008	"
27	1.962	4.313	"
28	1.962	4.618	"
29	1.962	4.923	"
30	1.962	5.228	"

TABLE B2. Inductance on Half of an Element
(Total inductance is twice that listed)

ELEMENT	NO. TURNS	DIAMETER	LENGTH	INDUCTANCE
23	2	1.25 (inches)	0.25 (inches)	0.20 (inches)
24	4	1.25	0.5	0.60
25	6	1.25	0.75	1.125
26	9	1.25	1.25	1.762
27	12	1.25	1.50	2.70
28	13	2.0	2.0	5.85
29	13	2.0	2.5	5.07
30	16	1.25	2.5	3.20

After results had been obtained with the computer model some differences were found between the assumed model and the actual antenna. Most important, the antenna includes an additional emement in a plane normal to that of the other elements. The element connects near the center of the transmission line and is directed toward the rear of the antenna at an angle of about 30 degrees with the transmission line. The purpose of this element is to eliminate transmission line resonances which would otherwise occur in the feed line due to the short circuit termination. Without the element the results from the model show a feed line resonance near 75 MHz. No attempt was made to include this additional element in the model. Since the element extends on only one side of the antenna, it would destroy the balance of the feed line to some extent and thus make questionable the ideal transmission line model. Explicit modeling of the transmission line wires could increase the computation time substantially.

The model was used to compute open circuit voltage at the source terminals by exciting the antenna with a 1 volt/m field incident from the forward direction. Input impedance and gain were also computed by applying a voltage source to the input. From these data the voltage across a 50-ohm load was computed, since this is the parameter of interest when the antenna is used for measuring field strength. The voltage on a 50-ohm load when a field of 1 volt/m is incident from the forward direction is plotted in Figure B2. Results were computed at 1 MHz intervals from 10 to 58 MHz and in larger intervals outside of this range. The number of segments in the model was increased for frequencies above 50 MHz to maintain accuracy in the solution. This is the cause of the discontinuity in the curve from 50 to 55 MHz. In general, the voltage shows the expected inverse frequency dependence from near the expected minimum operating frequency at 20 MHz to 100 MHz.

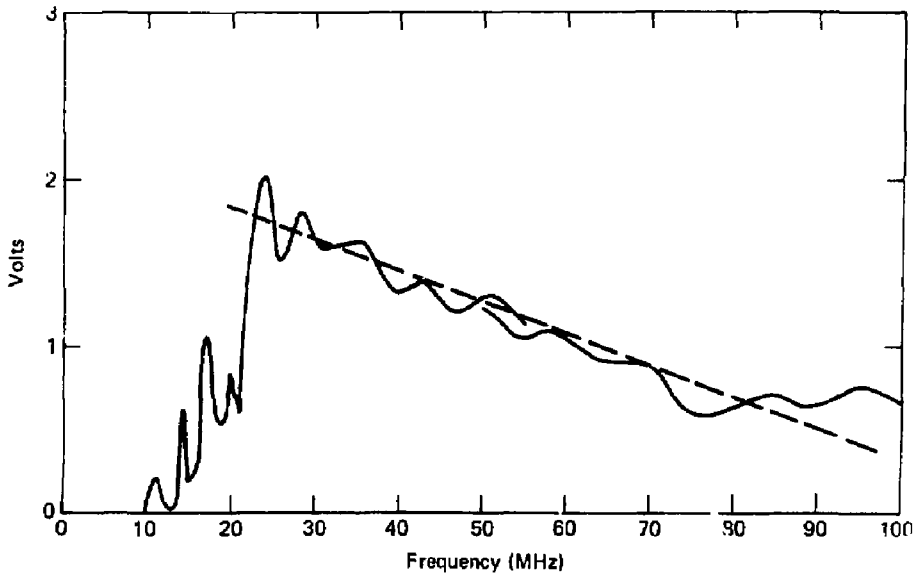

FIGURE B2 Magnitude of Voltage Across a 50 Ohm Load with 1 V/m-Hz Incident Field

Input impedance is plotted in Figure B3 and the VSWR for a 50-ohm load in Figure B4. The VSWR is in the general range of the data supplied by the manufacturer (American Electronics Lab.) but shows much more variation. This may be due to transmission line effects without the element to suppress resonances, or the AEL data may have been smoothed. The computed gain in Figure B5 is also in general agreement with AEL data.

References

1 - Numerical Electromagnetics Code (NEC) - Method of Moments, G. J. Burke, A. J. Poggio, NOSC/TD116, July 1977.

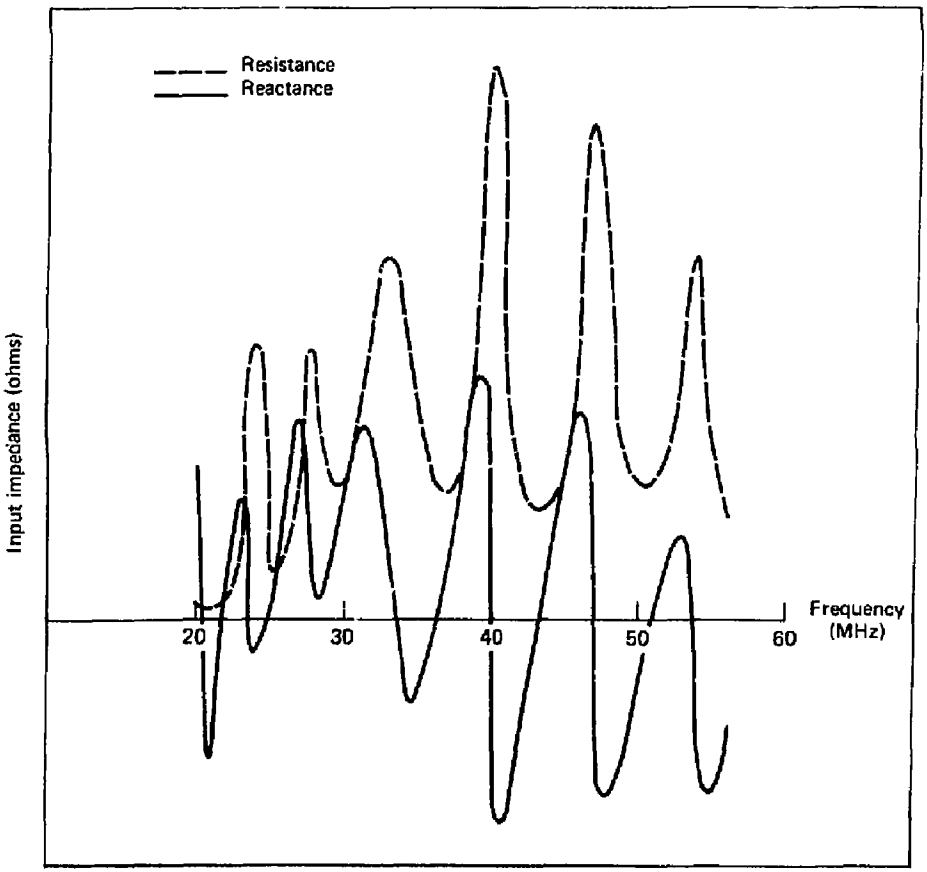

FIGURE B3 Input Impedance of 30-Element LP Antenna

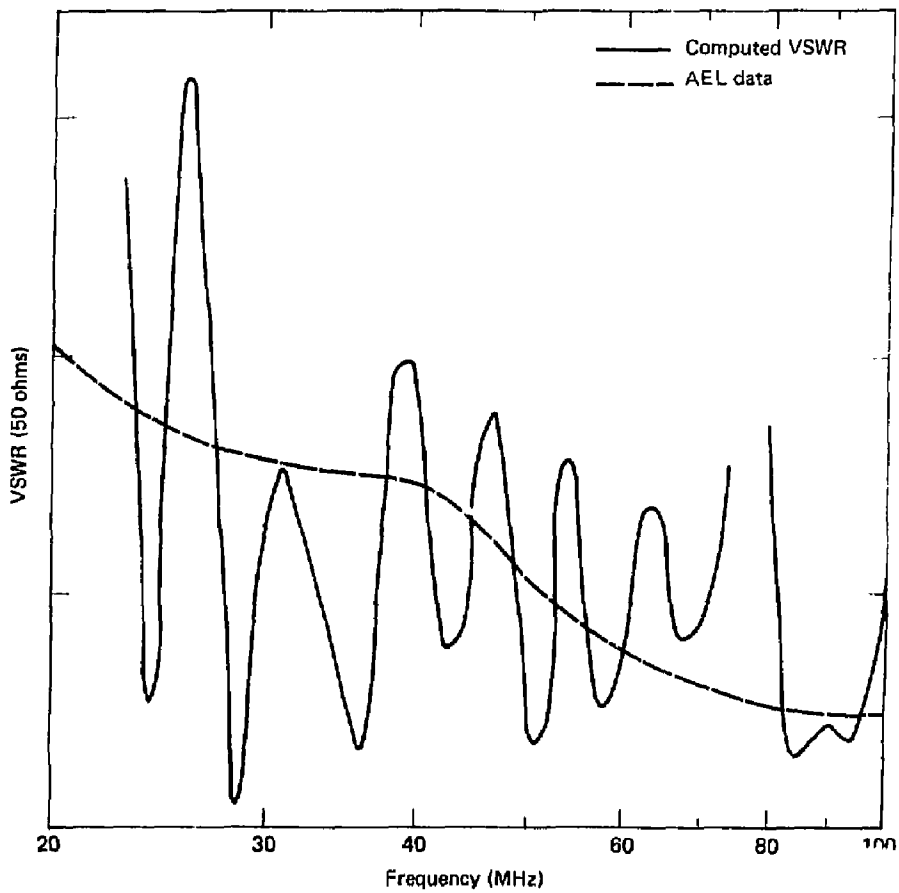

FIGURE B4 VSWR of 30-Element LP Antenna

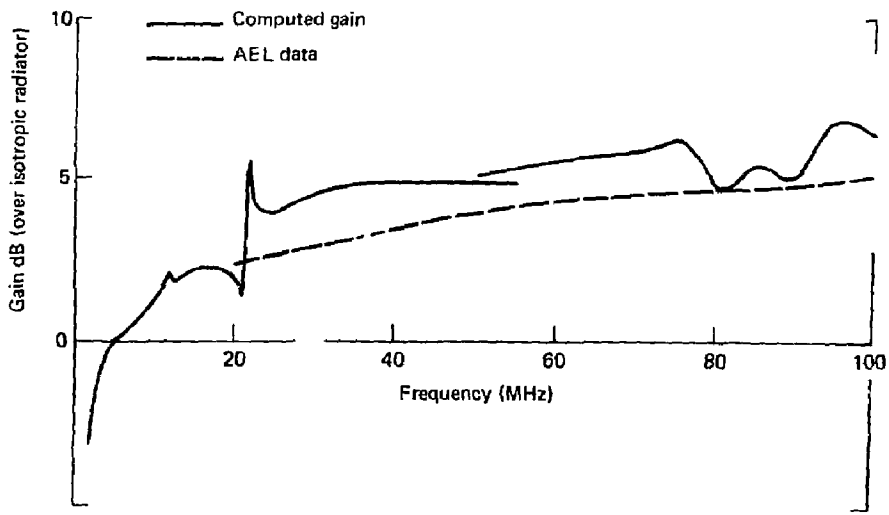

FIGURE B5 Gain of 30-Element LP Antenna

APPENDIX C

Sensor Locations

In this Appendix, the locations of the probes will be indicated with sketches. The same numbering system as in Section 4 for designating probes will be followed:

P1: EG&G Electric Field Probe

P2: LLL Monopole Probe

P3: LLL Active Antenna

P4: Log-Periodic Antenna

P5: EG&G Magnetic Field Probe

P6: Loop Antenna

P7: Cable Current Probe

A plan view of the building and all probe locations are shown in Figure C1. The free space time of flight between the probes are also indicated. In Figure C2, a sketch of the cathode end of the accelerator is shown with exact locations of probes P2 and P5 indicated. An enlarged view of the target end showing the location of P1 is sketched in Figure C3. In Fig. C4, the locations for the active antenna and the loop are indicated.

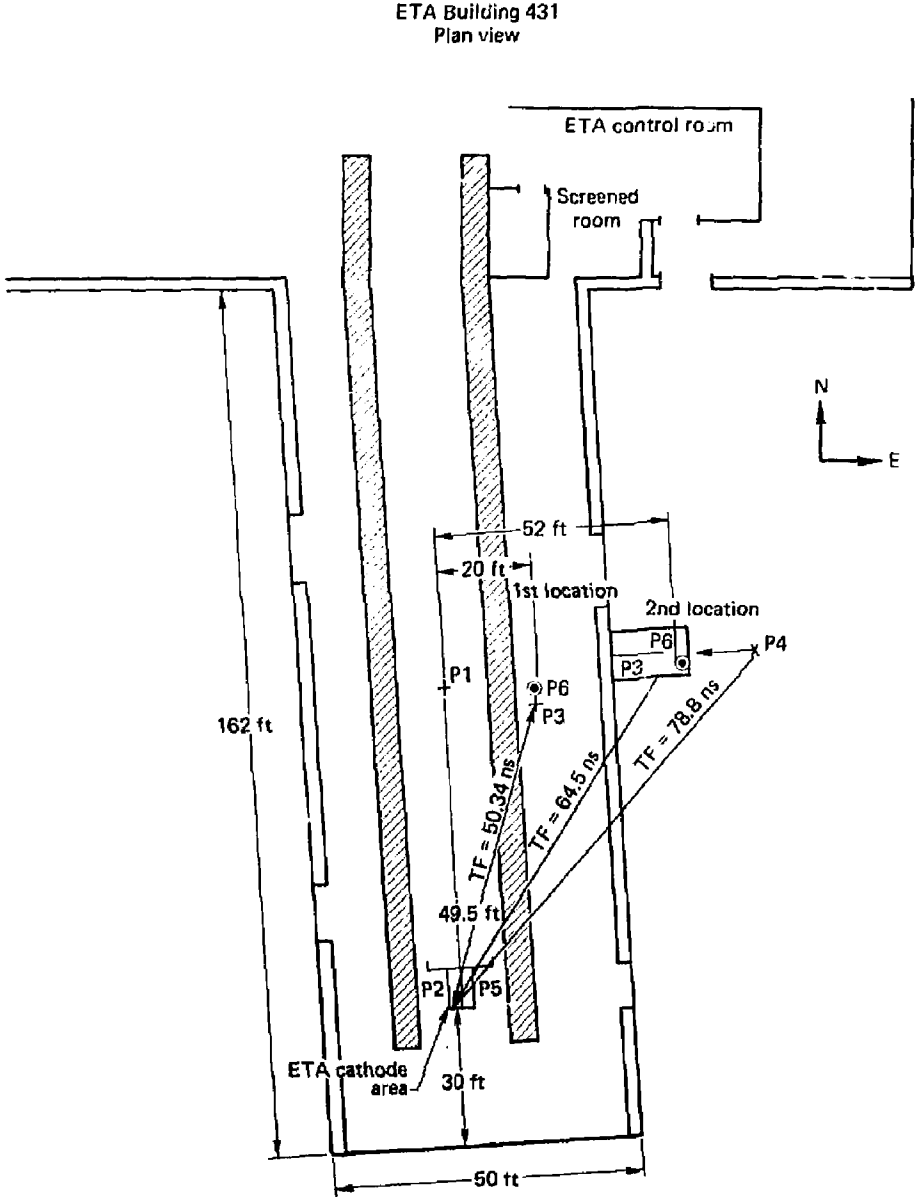

FIGURE C1 Plan View of ETA Building and Probe Locations

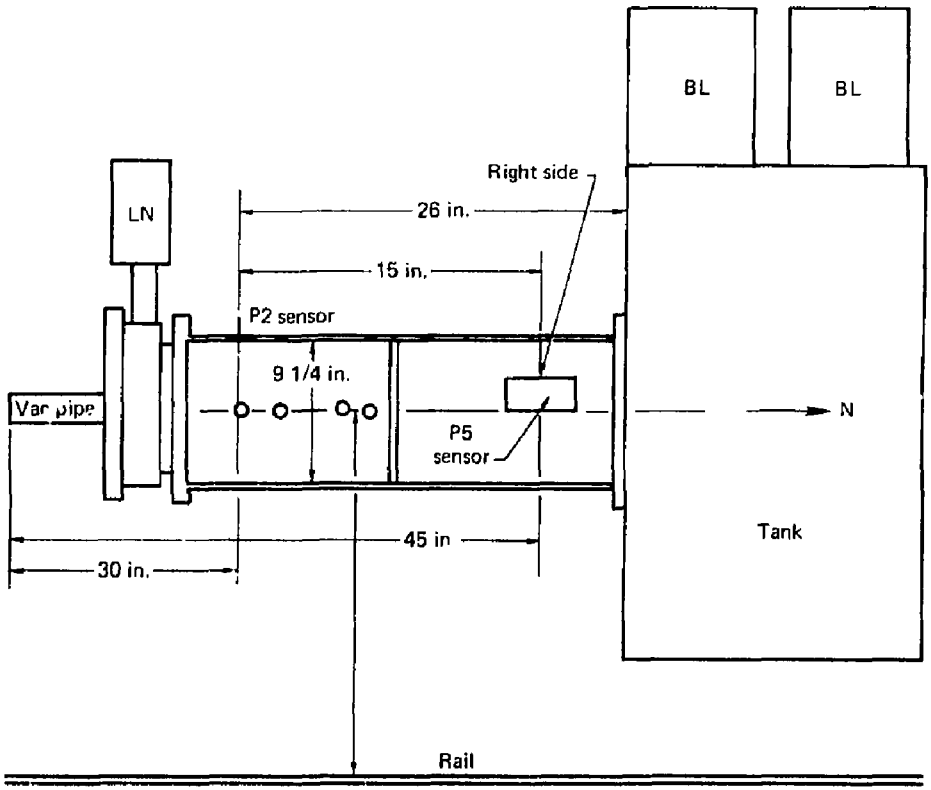

FIGURE C2 ETA Sketch - Cathode End of Accelerator

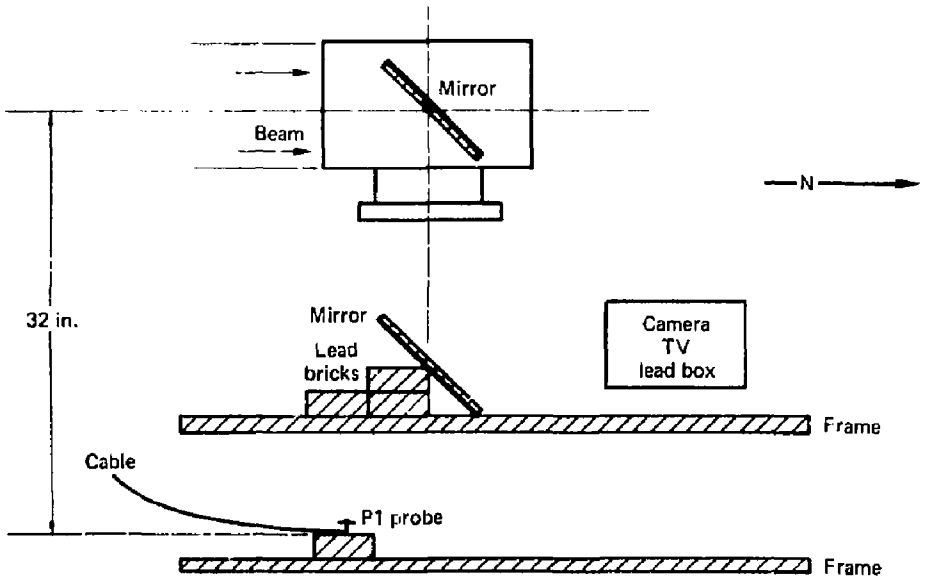

FIGURE C3 Beam Target Area Showing EG&G Electric Field Probe

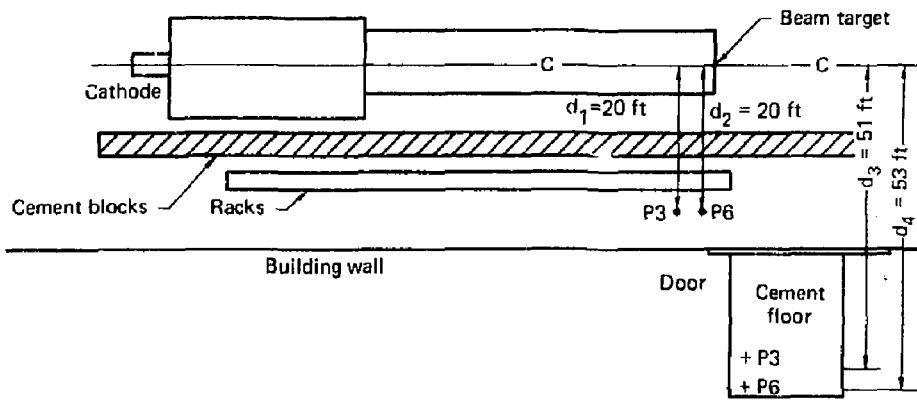

FIGURE C4 Sketch Showing Locations of LLL Active Antenna and Loop Probes

APPENDIX D

Data Acquisition and Processing

The software for data acquisition and manipulation is written using SPS BASIC.[1] This language includes software driver routines designed for use with the Tektronix R7912 transient digitizer.[2] This version of BASIC also includes signal processing and graphics routines to simplify data analysis.

The transient digitier utilizes a 512 by 512 matrix of diodes as a target for a writing beam similar to an oscilloscope. A scanning (or reading) beam looks at the activated diodes and digitizes the locations into a semiconductor memory. The system for data acquisition that was used is shown in Figure D1.

Acquisition of Data - The data is collected from the transient digitizer's memory in raw form (Figure D2). The raw data consists of the locations of waveform points on a diode matrix target and the appropriate scale factors. The blank diode matrix is read to identify any bad locations (defects). These defects are later eliminated from the raw data. The defect-corrected data is corrected for lens geometry distortion.[2] Geometry correction is done by comparing an experimentally acquired graticule against an ideal graticule and computing the appropriate correction factors. The final waveform is then normalized to a ground referenced potential. The waveform is graphed by linearly interpolating between each pair of points to achieve a continuous waveform trace. Figure D3 shows an example of the final trace.

We also have the capability to average together a number of traces. The average can be taken of up to 16,383 traces with an increase in collection time as the number of traces to be averaged increases. Signal-to-noise ratio will be improved by a factor of $\sqrt{\mu}$ where μ is the number of traces.

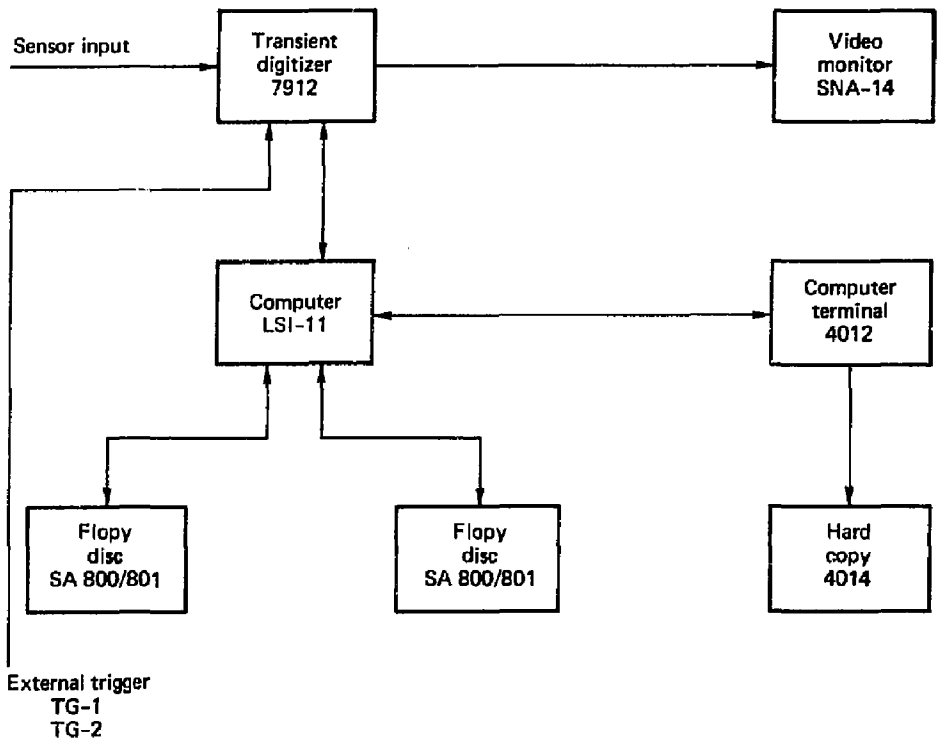

FIGURE D1 Block Diagram of Data

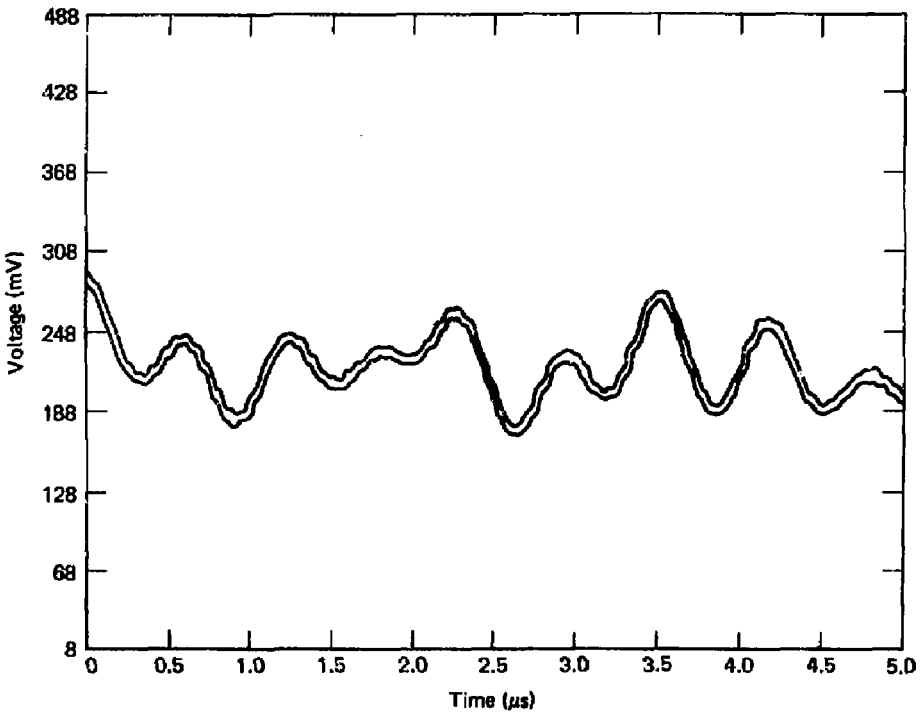

FIGURE D2 Example of Raw Data

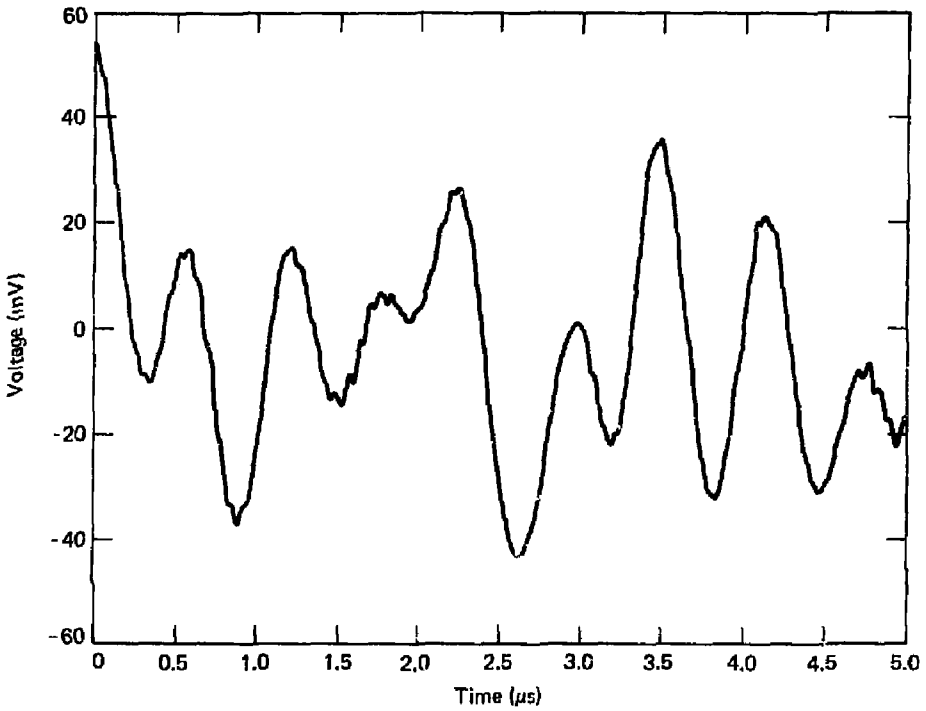

FIGURE D3 Example of Corrected Data

The final waveforms are stored on a floppy disc mass storage device. Up to 96 traces can be stored on a single floppy disc. Once a disc is filled with data, a backup of information is made by duplicating the data onto another disc.

Data Analysis - Once the data has been stored on a floppy disc an analysis can be made at one's leisure. Any portion of any waveform can be displayed. An expanded view of the first half of the example waveform is shown in Figure D4.

The waveform's spectra may be analyzed by computing the discrete Fourier transform. Figure D5 shows the magnitude of the discrete Fourier transform of the example waveform. Experimentation with windowing the time-domain data was performed to reduce spectral spreading in the frequency-domain. The Figures D6, D7, and D8 show the discrete Fourier transform of the example waveform after it has been windowed by the triangle, hamming, and hanning windows, respectively.[3]

After the data is in the frequency-domain, it is calibrated by using the transfer function for the antenna from which the data was collected.

Appendix E contains the complete listings of the programs that were used in processing data.

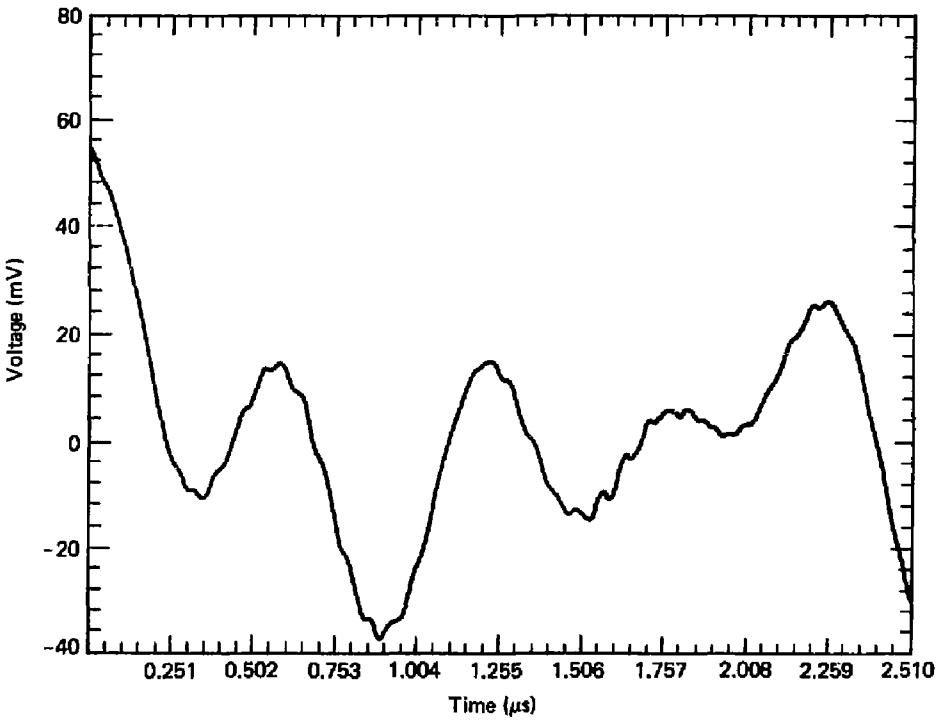

FIGURE D4 Example of Corrected Data

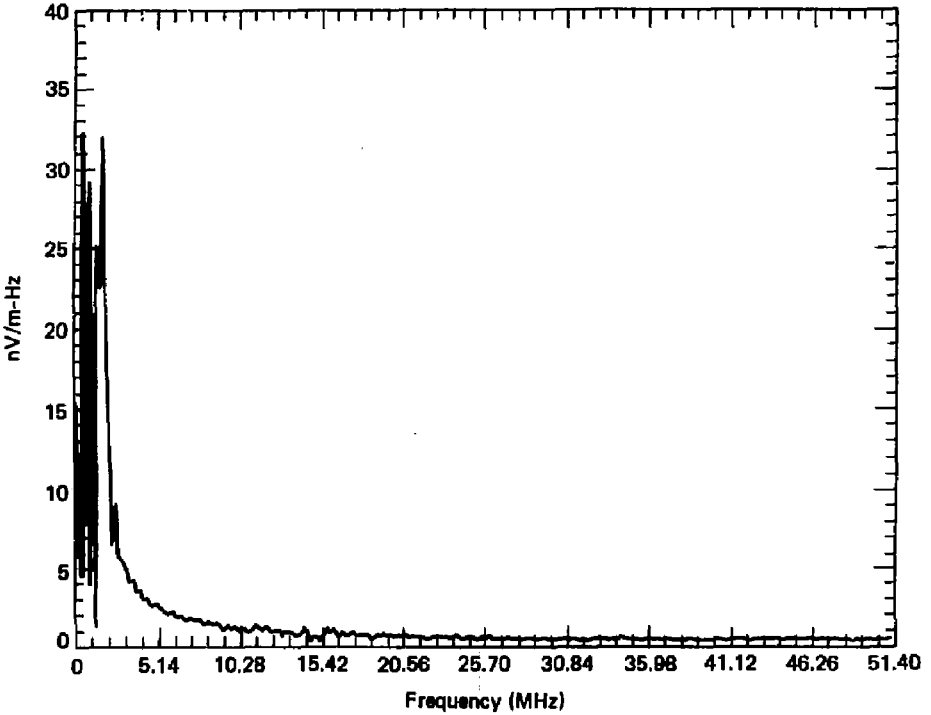

FIGURE D5 Rectangular Window Data

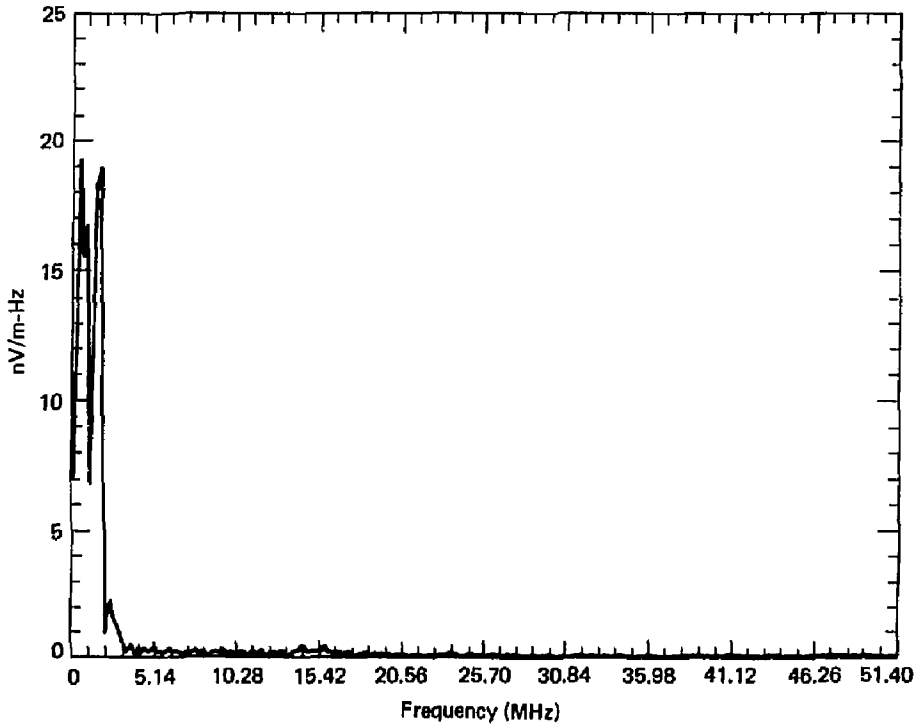

FIGURE D6 Triangular Window Data

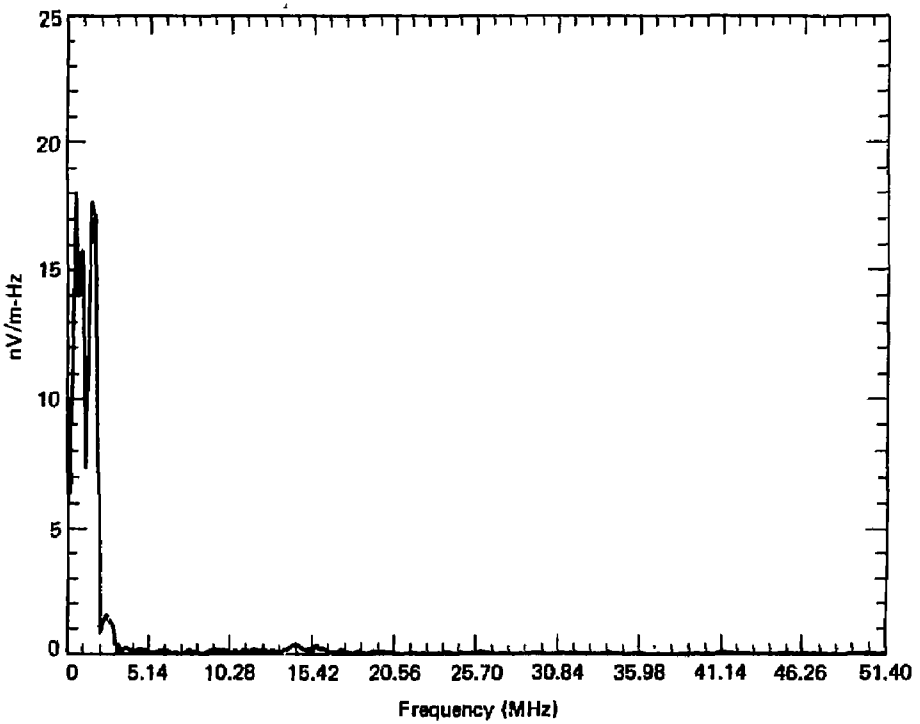

FIGURE D7 Hamming Windowed Data

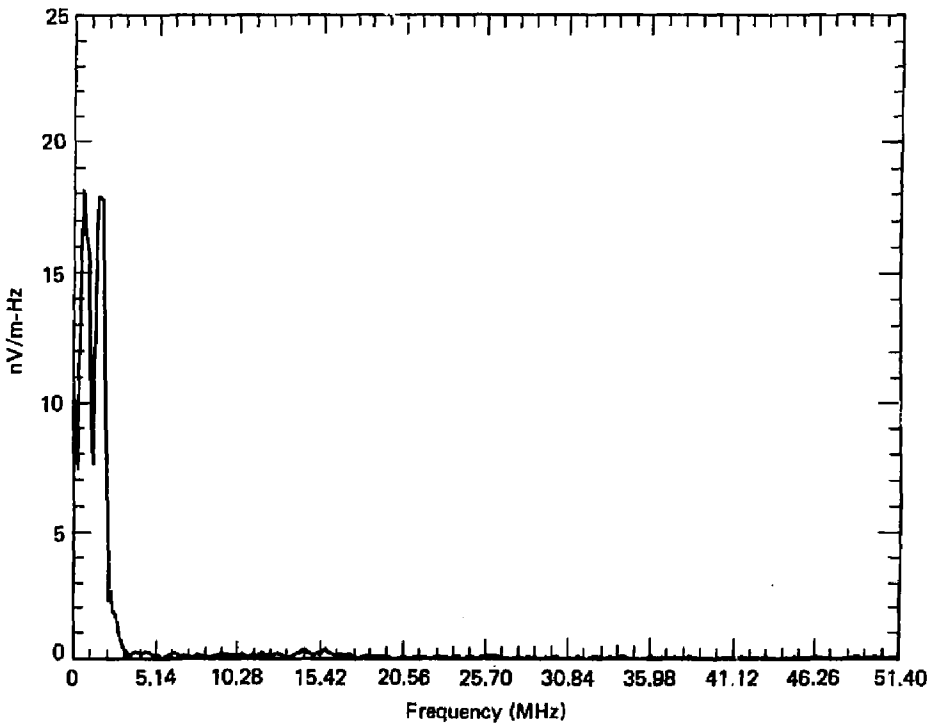

FIGURE D8 Hamming Windowed Data

Triggering and Final Time of Flights - The timing scheme and the point at which the data signals are collected are defined here. In order to make a determination of the signal characteristics, the data should appear soon after the receiving device (transient digitizer) has been activated by a triggering mechanism. This triggering was chosen to coincide with the charging and discharging of the Blumlein. The first trigger was placed at a position before the charging of the Blumlein. The charging takes from 20 - 22.5 μs in time. At a time 22.5 μs after the first trigger, the Blumlein is discharged. A firing trigger has been placed at this time. Shortly after the final trigger, the spark gaps are fired which induce the voltage across the accelerating cavity forming the beam. The beam takes about 300 ns to reach the target.

The time in which it takes the data signal to travel through the air, to the antenna sensor, and to the receiving transient digitizer were measured. This allows for a correlation of the collected data with the timing sequence precisely. The data signal is therefore delayed in reaching the transient digitizer by a short time interval. The delays for the sensors are given in the table below (for physical locations of probes, refer to Appendix C).

SIGNAL DELAY LIST*

SENSOR	DELAY TIME (ns)
EG&G Magnetic Field Sensor	208.5
EG&G Electric Field Sensor	208.5
Log-Periodic	320.8
Loop (1st Location)	200.3
LLL Active Antenna (1st Location)	215.3
Loop (2nd Location)	235.9
LLL Active Antenna (2nd Location)	235.9
Current Probe	240.0

*91 ns must be subtracted from these times due to trigger time-of-flight.

REFERENCES

1) Tektronix SPS BASIC Instruction Manual, Tektronix, November 1976.

2) Tektronix SPS BASIC R7912 Driver Package Instruction Manual, Tektronix, 1976.

3) Stanley, W. D., Digital Signal Processing, Reston Publishing Co., 1975.

APPENDIX E

Listing of Programs

```
LIST
10 PAGE
20 CLEAR
30 REM PROGRAM TO ACQUIRE A GEOMETRY CORRECTED TRACE
40 REM CORRECTED FOR ZERO-REFERENCE AND DEFECTS
50 LOAD 'TD'\ATTACH #1 AS TD7:
60 PUT 'NOD','TV' INTO #1
70 PAGE
80 PRINT 'TO IDENTIFY DEFECTS, TURN DOWN BEAM INTENSITY'
90 PRINT 'PRESS 'RETURN' WHEN READY'
100 WAIT\PAGE
110 DELETE DE\DEFECT #1,DE,10\RELEASE 'DEFECT'
120 PUT 'DOT','TV' INTO #1
130 PRINT 'TO INSTALL GEOMETRY CORRECTION, TURN DOWN BEAM INTENSITY'
140 PRINT 'ADJUST GRATICULE INTENSITY AND PRESS 'RETURN'"
150 WAIT\PAGE
160 PUT 'STO' INTO #1
165 DELETE R,P,H,V
170 GET R,P FROM #1,'RAU'
180 INSTALL R,P,H,V\RELEASE 'INSTALL'
190 PUT 'TV','NOD' INTO #1
200 PRINT 'TO ACQUIRE ZERO-REFERENCE TRACE, GROUND INPUT'
210 PRINT 'ADJUST BEAM INTENSITY, POSITION TRACE, & PRESS 'RETURN'"
220 GOSUB 580
230 ZREF C,D,Z\RELEASE 'ZREF'
240 DELETE C,UC,$C,HC$,VC$,D,UD,SD,HD$,VD$
250 PUT 'TV' INTO #1
260 PRINT 'TO ACQUIRE WAVEFORM TRACE, UNGROUND VERTICAL PLUG-IN'
270 PRINT 'INPUT WAVEFORM,ADJUST INTENSITY & PRESS 'RETURN'"
280 GOSUB 580
290 DELETE P,UP,$P,HP$,VP$
300 DELETE E,WE,$E,HE$,VE$
310 WAVEFORM E IS WE(511),$E,HE$,VE$
320 GET VS FROM #1,'VS1'
330 NORMAL C,D,E,Z,VS\RELEASE 'NORMAL'
340 DELETE C,UC,$C,HC$,VC$,D,UD,SD,HD$,VD$
350 PRINT 'TYPE FILE NAME'
360 INPUT Z$
```

```
LIST
10 PAGE
20 PRINT 'INPUT FILE NAME'
30 INPUT U$
40 OPEN #2 AS DX1:U$ FOR READ
50 DELETE T
60 WAVEFORM T IS TA(511),TD,HTS,VTS
70 READ #2,RS,T
80 CLOSE #2
90 DELETE BB,UB,DB,HBS,VBS
100 PAGE
105 PRINT 'GRAPH LIMITS ARE IN RANGE OF 0 TO 511'
110 PRINT 'INPUT LOWER GRAPH LIMIT'
120 INPUT M
130 PRINT 'INPUT UPPER GRAPH LIMIT'
140 INPUT N
145 WAVEFORM BB IS UB(N),DB,HBS,VBS
150 LET HBS=HTS
160 LET VBS=VTS
170 LET DB=TD
180 UB(M:N)=TA(M:N)
190 PAGE
193 LET FH=1/(2*DB)
194 LET FM=1/(512*DB)
195 PRINT RS
196 PRINT 'MINIMUM FREQUENCY IS';FM;'HZ  MAXIMUM FREQUENCY IS';FH;'HZ'
200 GRAPH BB
210 WAIT\PAGE
220 PRINT 'DO YOU WANT TO REDISPLAY GRAPH'
230 INPUT Q$
240 IF Q$='Y' THEN GOTO 90
250 END

READY
$
```

```
LIST
10 REM PROGRAM TO READ WAVEFORM FROM DISK 1
20 REM JOHN E. ZICKER 9-20-79
30 PAGE
40 PRINT 'TYPE FILE NAME'
50 INPUT A$
60 DELETE E,WE,DE,HE$,VE$
70 DELETE BB,WB,DB,HB$,VB$
80 DELETE CC,WC,DC,HC$,VC$
90 WAVEFORM E IS WE(511),DE,HE$,VE$
100 WAVEFORM BB IS WB(256),DB,HB$,VB$
110 WAVEFORM CC IS WC(256),DC,HC$,VC$
120 OPEN #2 AS DX1:A$ FOR READ
130 READ #2,R$,E
140 CLOSE #2
150 RFFT E,BB,CC
160 POLAR BB,CC
170 PRINT 'INPUT LOWER GRAPH LIMIT'
171 DELETE L,T
172 INPUT L
173 PRINT 'INPUT UPPER GRAPH LIMIT'
175 INPUT T
180 DELETE YY,WY,DY,HY$,VY$
190 WAVEFORM YY IS WY(T),DY,HY$,VY$
200 WY(L:T)=WB(L:T)
210 LET DY=DB
220 LET HY$=HB$
230 LET VY$=VB$
240 PAGE
241 LET FH=1/(512*DE)
242 LET FH=1/(2*DE)
245 PRINT R$
246 PRINT 'MINIMUM FREQUENCY IS';FH;'HZ  MAXIMUM FREQUENCY IS';FH;'HZ'
250 GRAPH YY\RELEASE 'GRAPH'
260 WAIT\PAGE
270 PRINT 'DO YOU WANT TO REDISPLAY GRAPH'
280 INPUT G$
290 IF G$='Y' THEN GOTO 170
```

```
300 RELEASE ALL
310 END

READY
*
```

```
370 PRINT 'TYPE TITLE'
380 INPUT $$
390 ONERR IA GOTO 500
400 OPEN $2 AS DX1:Z$ FOR WRITE
410 WRITE $2,$$,E
420 CLOSE $2
430 PAGE\PRINT $$
440 LET FQ=1/(512*SE)
450 LET FH=1/(2*SE)
460 PRINT 'MINIMUM FREQUENCY IS';FQ;'HZ  MAXIMUM FREQUENCY IS';FH;'HZ'
470 GRAPH E\RELEASE 'GRAPH'
480 WAIT\PAGE
490 PUT 'TV' INTO $1
500 PRINT 'DO YOU WANT TO RERUN'
510 INPUT Q$
520 IF Q$='Y' THEN GOTO 260
530 DETACH $1
540 RELEASE 'TD'
550 RELEASE ALL
570 END
580 WAIT\PAGE
590 RELEASE 'PAGE','CLEAR'
600 PUT 'STO' INTO $1
610 DELETE R,P
620 INTEGER WP(511)
630 WAVEFORM P IS WP,$P,HP$,VP$
640 GET R,P FROM $1,'RAW'
650 REJECT R,P,DE\RELEASE 'REJECT'
665 DELETE A,B,WA,$A,HA$,VA$,WB,$B,HB$,VB$
680 INTEGER WA(511)\INTEGER WB(511)
670 WAVEFORM A IS WA,$A,HA$,VA$
680 WAVEFORM B IS WB,$B,HB$,VB$
690 EDGE R,P,A,B\RELEASE 'EDGE'
700 DELETE R,P
710 DELETE C,WC,$C,HC$,VC$
720 WAVEFORM C IS WC(511),$C,HC$,VC$
730 MAP A,C,H,V
735 RELEASE 'MAP'
```

```
740 DELETE A,WA,SA,HAS,VAS
750 WAVEFORM D IS WD(511),SD,HD$,VD$
760 MAP D,D,H,V\RELEASE 'MAP'
770 DELETE D,WD,SD,HDS,VDS
780 DELETE A,WA,SA,HAS,VAS
790 RETURN
800 PRINT IA
810 PRINT "DO YOU WANT TO RENAME FILE"
820 INPUT OOS
830 IF OOS="Y" THEN GOTO 350
840 END

READY
```